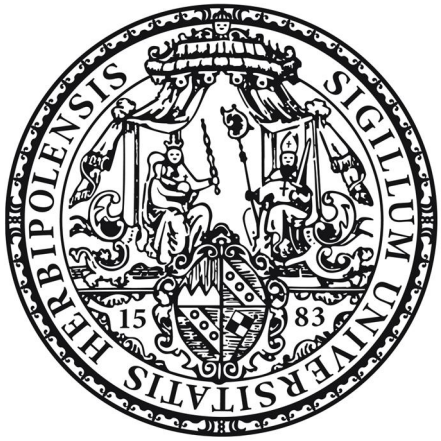

Establishing successful protocols and imaging pipelines for Expansion Microscopy in murine blood platelets

Etablierung erfolgreicher Protokolle zur Probenpräparation und Bildgebung für die ‚Expansion Microscopy' in murinen Thrombozyten

Doctoral thesis for a medical doctoral degree
at the Graduate School of Life Sciences,
Julius-Maximilians-Universität Würzburg,
Section Biomedicine

submitted by

Max Aigner

from

Mutlangen, Germany

Würzburg 2022

Submitted on: ……

Office stamp

Members of the Thesis Committee:

Chairperson: Prof. Dr. Nicolas Schlegel

Primary Supervisor: Prof. Dr. Katrin Heinze

Supervisor (Second): Prof. Dr. Markus Sauer

Supervisor (Third): Prof. Dr. Harald Schulze

Date of Public Defence: ……

Date of Receipt of Certificates: ……

Summary

Platelets play an important role in the body, since they are part of the hemostasis system, preventing and stopping blood loss. Nevertheless, when platelet or coagulation system function are impaired, uncontrolled bleedings but also irreversible vessel occlusion followed by ischemic tissue damage can occur. Therefore, understanding platelet function and activation, mechanisms which are controlled by a variety of platelet membrane receptors and other factors is important to advance out knowledge of hemostasis and platelet malfunction. For a complete picture of platelet function and their modulating behavior it is desired to be able to quantify receptor distributions and interactions of these densely packed molecular ensembles in the membrane. This challenges scientists for several reasons. Most importantly, platelets are microscopically small objects, challenging the spatial resolution of conventional light microscopy. Moreover, platelet receptors are highly abundant on the membrane so even super-resolution microscopy struggles with quantitative receptor imaging on platelets.

With Expansion microscopy (ExM), a new super-resolution technique was introduced, allowing resolutions to achieve super-resolution without using a super-resolution microscope, but by combining a conventional confocal microscopy with a highly processed sample that has been expanded physically. In this doctoral thesis, I evaluated the potential of this technique for super-resolution platelet imaging by optimizing the sample preparation process and establishing an imaging and image processing pipeline for dual-color 3D images of different membrane receptors. The analysis of receptor colocalization using ExM demonstrated a clear superiority compared to conventional microscopy. Furthermore, I identified a library of fluorescently labeled antibodies against different platelet receptors compatible with ExM and showed the possibility of staining membrane receptors and parts of the cytoskeleton at the same time.

Zusammenfassung

Thrombozyten spielen eine wichtige Rolle im Körper, denn als Teil des Gerinnungssystems, sind sie daran beteiligt Blutverlust vorzubeugen und zu stoppen. Gleichwohl können sie bei Störungen des Gerinnungssystems zu unkontrollierbaren Blutungen und auch durch Aggregation zu kardiovaskulären Ereignissen, wie Herzinfarkt und Schlaganfällen führen. Für ein besseres Verständnis von Hämostase und Gerinnungsstörungen ist es deshalb nötig die Funktion und Aktivierung von Thrombozyten zu verstehen, welche durch eine Vielzahl von Membranrezeptoren und anderen Faktoren gesteuert wird. Eine Methode, um weitere Einblicke in diese Prozesse zu bekommen ist die mikroskopische Darstellung von Rezeptorverteilungen auf der Zellmembran und deren Interaktionen. Dies zu realisieren ist aus verschiedenen Gründen anspruchsvoll. Der mikroskopisch kleine Durchmesser der Thrombozyten macht es konventioneller Lichtmikroskopie schwer, einzelne Rezeptoren auf der Membran darzustellen. Außerdem befinden sich sehr viele Rezeptoren dicht gepackt auf der Membran, sodass sogar superhochauflösende Mikroskope Schwierigkeiten haben, die Rezeptoren quantitativ zu beurteilen.

Mit ‚Expansion microscopy' (ExM) wurde eine relativ junge superhochaufösende Technik auf Thrombozyten angewendet. Diese Technik erreicht Auflösungen vergleichbar mit sogenannten ‚super-resolution' Mikroskopen, ohne die Benutzung selbiger, sondern durch die Kombination von konfokaler Mikroskopie mit einer physikalisch expandierten Probe. In dieser Arbeit evaluierte ich das Potential dieser Technik für superhochauflösende Bilder von Thrombozytenrezeptoren und optimierte die Probenvorbereitung, sodass zweifarbige 3D Bilder von verschiedenen Membranrezeptoren möglich waren. Die Ergebnisse der Kolokationsanalyse zeigten einen deutlich vergrößerten Dynamikumfang durch ExM. Außerdem katalogisierte ich fluoreszenzmarkierte Antikörper gegen verschiedene Thrombozyten Rezeptoren bezüglich ihrer Tauglichkeit mit ExM und zeigte, dass es möglich ist Membranrezeptoren und Bestandteile des Zytoskeletts gleichzeitig zu färben.

Content

Abbreviations

AB	Antibody
A488	Alexa Fluor 488
A594	Alexa Fluor 594
AcX	Acryloyl-X
ADP	Adenosine diphosphate
APS	Ammonium persulphate
BSA	Bovine serum albumin
CHO-cells	Chinese hamster ovary cells
CS-Buffer	Cytoskeleton buffer
ddH2O	Double-distilled water
DMAA	N,N-dimethylacrylamide
DMEM	Dulbecco‘s Modified Eagle Media
ECM	Extracellular matrix
EDTA	Ethylenediaminetetraacetic acid
EGTA	Ethylene glycol-bis(β-aminoethyl ether)N,N,N',N'-tetraacetic acid
ExM	Expansion microscopy
FACS	Fluorescence-activated cell sorting
GFP	Green fluorescent protein
GP	Glycoprotein
HEPES	4-(2-hydroxyethyl)-1-piperazineethanesulfonic acid
KO	Knockout
KPS	Kalium persulfate
MES	2-(N-Morpholino)-ethansulfonsäure
MFI	Mean fluorescent intensity
MPV	Mean platelet volume
NA	Numerical aperture
NaCl	Sodium chlorite
PALM	Photoactivated localization microscopy
PBS	Phosphate buffered saline
PCC	Pearson correlation coefficient
PFA	Paraformaldehyde
PGI2	Prostacyclin
PLP	Periodate-lysine-paraformaldehyde
proExM	Protein retention microscopy
PRP	Platelet-rich plasma
PSF	Point spread function
px	Pixel
RCM	Re-scan confocal microscopy
rpm	Revolutions per minute
RT	Room temperature
SDS	Sodium dodecyl sulfate
SIM	Structured Illumination Microscopy

STED	Stimulated emission depletion microscopy
STORM	Stochastic optical reconstruction microscopy
TEMED	Tetramethylethylenediamin
TF	Tissue factor
Tx	Thromboxane
U-ExM	Ultrastructure expansion microscopy
vWF	von Willebrand Factor
WT	Wildtype
x10-ExM	X10 Expansion microscopy

1 Introduction

Blood platelets play an important role in different processes in the human body, such as hemostasis, thrombosis, inflammation, and cancer genesis [1]. Densely packed on the platelet membrane, a large number of receptors are controlling the activation, interaction, and recruitment of platelets. With the classical activation pathway being highly investigated, there is still a lack of insight into receptor distribution and their interactions. Little is known for example about the behavior of the receptor Glycoprotein (GP) Ibα, which shows effects apart from classical agonist-induced signaling pathways, which could be linked to receptor dimerization and changes in receptor distribution on the platelet surface or within the cytosol and the membrane [2]. For a complete picture of platelet function and their modulating behavior therefore it is desired to be able to quantify receptor distributions and visualize the interactions of these densely packed molecular ensembles in the membrane themselves but also with intracellular components like the actin filament.

The imaging of receptor distribution or dynamics on the platelet membrane is challenging mostly due to two reasons. Firstly, platelets are relatively small with a diameter of 1-4 µm (in mice) [3] and secondly, the platelet receptors are highly abundant on the membrane [4], making it hard to image single receptors or even their distribution.

Today, scientists can choose between a lot of different microscopy techniques. However, diffraction-limited techniques like confocal fluorescent microscopy with a lateral resolution of around 250 nm, do not provide a resolution close to the receptor level [5]. To achieve the required resolution, scientists need to use techniques from the super-resolution field, like ‘Structured Illumination Microscopy’ (SIM) or ‘Stochastic Optical Reconstruction Microscopy’ (STORM), which allow the visualization of cell architecture down to the single molecule level but often include extensive image processing/ reconstruction and/or effortful sample preparation with a limited choice of fluorophores. Furthermore, these methods are mostly more expensive, especially when imaging is done in 3D and multicolored [5]–[7].

In the year 2015, the laboratory of Edward Boyden published a new super-resolution method called Expansion Microscopy (ExM), which allows super-resolution, by physically expanding the sample with the help of a swellable hydrogel and subsequently imaging it on a conventional fluorescent microscope. Hereby, the

effective resolution (both in the lateral and axial direction) can be increased 4-fold [8]. The major bottleneck of the ExM approach is the intensity loss due to digestion and expansion. Furthermore, an isotropic expansion must be guaranteed to avoid distortions and the protocol needs to be adjusted to different samples, because different tissues/specimens require different treatment. To validate the performance of ExM regarding 3D imaging of murine blood platelet receptor distribution and their colocalization analysis, the different steps of the ExM protocol (regarding fixation, labeling, linking, gelation, digestion, expansion, and imaging) need to be optimized for platelets and an imaging and image processing pipeline needed to be developed.

1.1 Blood platelets

Platelets are small anucleated, discoid shaped cell fragments, released as so called proplatelets into the blood circulation by megakaryocytes in the bone marrow. Shear forces in the blood stream induce fragmentation of proplatelets into platelets [9]. With a dimeter of 1-4 µm in mice [3], platelets are the smallest cells in blood. A stable platelet count of approximately 1,100,000/µl in mice [10] (150,000-450,000/µl in humans [11]), is maintained by the reticuloendothelial system of liver and spleen, which remove aged platelets from the circulation approximately after 5 days in mice and 10 days in humans [12]. Platelets are the key cells of primary hemostasis and thrombosis but beyond an evolving role in regulation of inflammation and cancer genesis has been described [1].

In case of vessel damage, components of the extracellular matrix (ECM) are exposed and get in contact with platelet receptors. Complex intracellular signaling in combination with the release of soluble mediators lead to platelet activation and recruitment. To form a stable thrombus, platelets, which are responsible for the ‘primary hemostasis’, and the coagulation system, which is responsible for the ‘secondary hemostasis’, need to work together. The activation of the coagulation system, respectively coagulation cascade, can be initiated over two pathways: Extrinsically over locally exposed tissue factor (TF) or intrinsically by the activation of coagulation factor (F)XII [2]. When the coagulation system is activated, thrombin is formed. This leads to the conversion of fibrinogen to fibrin, which is responsible for the stability of the thrombus. Furthermore, the formation of soluble thrombin induces strong platelet activation and aggregation. Without these processes, normal hemostasis is impossible [2]. When primary or secondary hemostasis are dysregulated, uncontrolled bleedings like in hemophilia, but also irreversible vessel occlusion, like in myocardial

infarction or stroke, followed by ischemic tissue damage can occur. Not only because these two health incidents are very common causes for death worldwide, a better understanding of platelet function is of big interest for researchers [13] [2].

1.1.1 Platelet activation and thrombus formation

The process of platelet activation can be divided into three major steps: tethering, activation, and firm adhesion (**Figure 1**).

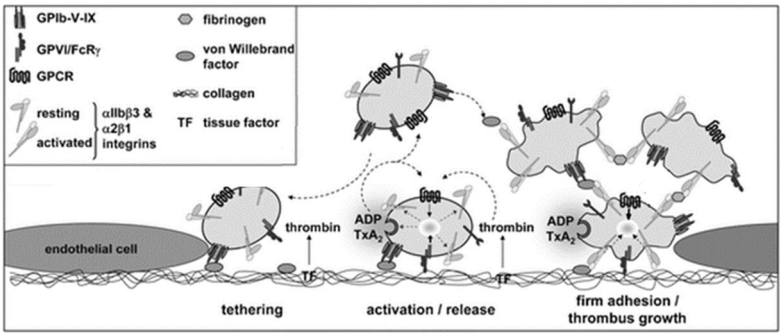

Figure 1: Model for platelet adhesion to the subendothelial matrix at sites of vascular injury and subsequent thrombus formation. GPIb-vWF interactions mediate the first contact (tethering) of the platelet to the ECM. The cellular activation is initiated by GPVI-collagen interactions, followed by the activation of integrins and release of secondary mediators. Finally, with the connection between integrins (e.g., GPIIb/IIIa (=αIIbβ3)) the firm adhesion to collagen is achieved. Adapted from Stegner et al., 2011 [2]

1. During tethering, the first contact to the injured vessel wall takes place through the membrane receptor Glycoprotein (GP) Ib/V/IX binding the von Willebrand Factor (vWF), which is exposed through the injury on the ECM. This interaction does not lead to firm adhesion to the vessel wall since it is transient and reversible, but it decelerates the platelets in the blood stream, what enables other receptors to get in contact with their ligands [14]. This effect is mainly important in arterioles and stenosed arteries, where high shear forces are present [15].
2. The next step in thrombus formation is mediated through the binding of the major collagen receptor GPVI to exposed collagen [16]. This triggers a conformational change of integrin GPIIb/IIIa to its activated fibrinogen binding conformation and the release of secondary mediators from platelet α- and δ-granules [2]. These soluble mediators like thromboxane (Tx) A_2 or adenosine diphosphate (ADP) enhance the platelet activation and together with locally produced thrombin, lead to further platelet recruitment [15], [17].
3. Finally, adhesion is mediated by the binding between integrins and ECM proteins like collagen, laminin and fibronectin [15].

1.1.2 Platelet receptors

Located on the platelet membrane, different receptors modulate platelet activation and signal transduction. In the following section I will outline 3 of them more specifically.

1.1.2.1 Glycoprotein IIb/IIIa

Glycoprotein (GP) IIb/IIIa (also known as integrin αIIbβ3) is the most abundant platelet adhesion receptor with up to 120,000 copies per platelet [4]. Specific intracellular signals lead to a conversion of the integrin from a passive to an active state ('inside-out'-signaling). In the active state, GPIIb/IIIa binds to fibrinogen, fibrin and vWF, triggering cellular processes ('outside-in'-signaling), promoting cell spreading and clot retraction. Mutations in GPIIb/IIIa result in severe hemorrhagic disorders [2].

1.1.2.2 Glycoprotein VI

Glycoprotein (GP) VI is one of the major collagen receptors and belongs to the immunoglobulin (Ig) superfamily. Through intracellular signaling after collagen binding, GPVI initiates integrin activation and therefore cell adhesion and thrombus growth. Furthermore, the release of soluble agonists as ADP and TXA_2 is induced, also leading to further activation of integrins and of further platelets. In return, the GPVI-collagen induced platelet adherence is strengthened through integrin-mediated adhesion. Without intact GPVI function or GPVI deficiency, the initial platelet contact with collagen and the integrin activation are reduced, leading to improved protection from intravascular thrombosis with only moderately increased bleeding time in mouse models [18] [16]. Thus GPVI blockade is considered as potential and powerful.

1.1.2.2.1 Glycoprotein Ib-V-IX

The Glycoprotein (GP) Ib-V-IX complex is important for the initial contact with the damaged ECM (tethering) and consists out of the components GPIbα (2x), GPIbβ (2x), GPIX (1x) and GPV (1x) [19]. Being the major receptor for the vWF, GPIbα is involved in the adhesion of platelets and allows other receptors the interaction with their ligands (e.g., GPVI and collagen). Therefore, GPIb-V-IX is responsible for initial platelet recruitment and platelet activation. [4], [2]

GPIbα also plays a role in the clearance of platelets, since *in vivo* treatment of mice with monoclonal anti-GPIbα IgG antibodies (p0p 3-5), leads to severe and rapid platelet depletion (>98%) [20]. *In vitro*, the treatment of platelets with this antibody leads to 'non-classical' clotting, a kind of agglutination without the formation of filopodia (**Figure 2**) [20]. The mechanisms behind these processes are mediated apart from classical agonist-induced signaling pathways and could be induced by receptor

dimerization and changes in receptor distribution. ExM could help to image and understand these processes and also be an important part in the comprehension of the role of the connection between GPIbα and the platelets actin filament network [19].

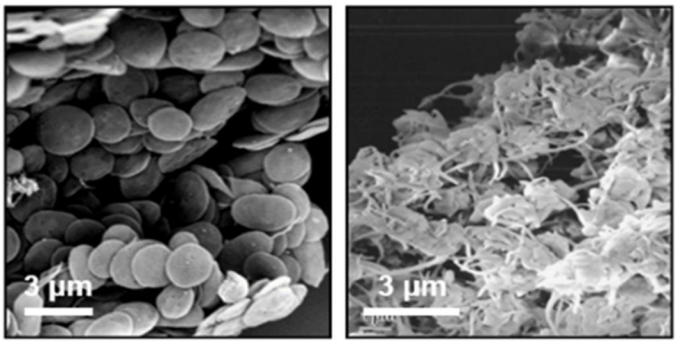

Figure 2: Anti-GPIbα antibodies induce non-classical clotting. Application of anti-GPIbα antibodies without mechanical stress leads to 'non-classical' platelet clotting (left). The platelets adhesiveness is elevated, but filopodia as normally observable in platelet aggregation (right) is not visible. Images with courtesy of Bernhard Nieswandt.

1.2 Fluorescence Microscopy and beyond

In present-day research microscopy is an indispensable tool to visualize processes of live otherwise inaccessible to the human eye. Over the years, many different methods were developed to magnify and examine previously hidden structures. With the first advanced optical microscopes built by Ernst Abbe and Carl Zeiss, the first 'resolution revolution' started, revolutionizing the way scientists could examine tissue architecture, infections and diseases [5]. These advanced optical microscopes are physically limited in resolution because of the diffraction limit as described by Abbe in 1873 [21]. With the second 'resolution revolution", new technologies were invented to overcome this limitation. Electron microscopy is able to resolve structures with a near-atomic resolution, but has the limitation that samples need to be highly processed or purified [22], [23]. Fluorescent microscopy allows the observation of single molecule interaction and dynamics in a physiological environment but is principally also limited to the diffraction limit [5]. Nevertheless, this limitation can be overcome through modern super-resolution techniques, including the young technique Expansion microscopy (ExM) [8]. In the following chapters I will outline the concept of resolution and its impact on super-resolution microscopy and the technique ExM in particular.

1.2.1 The concept of resolution

The first simple light microscopes used a light source and a lens system to show the researcher the magnified image in the ocular. The contrast of this image is created through variations in transparency of the sample [5].

Resolution power

Already Ernst Abbe described in 1873 that the achievable resolution with light microscopy is 'diffraction limited' by the laws of physics [21]. This is due to the fact, that the light emitted by a point emitter cannot be focused on an infinitely small spot on the image plane. As one of the basic characteristics of light is to have wave properties, this emitted light interferes at the image plane, creating a bright circle with dark and bright concentric rings around it (Airy pattern, **Figure 3.A**). This pattern created by a point emitter is called 'point spread functions' (PSF) [5], [24].

The resolution of a microscope is defined as the smallest distinguishable distance between two partially overlapping PSFs (**Figure 3.B**). The exact resolution d_{lim} can be calculated over the diameter of the Airy disk, which is the result of wavelength and

numerical aperture (NA) of the microscope and the refractive index of the sample medium ŋ [5]:

$$d_{xy} = \frac{\lambda}{2 * NA} \quad (1)$$

$$d_z = \frac{2\lambda\eta}{(2 * NA)^2} \quad (2)$$

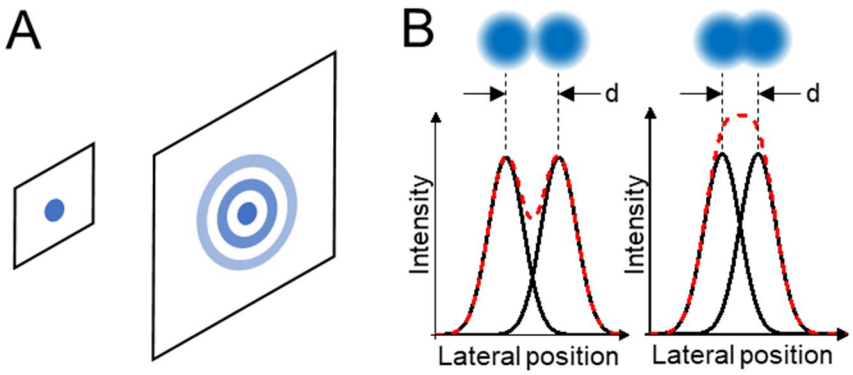

Figure 3: Airy pattern produced by a point emitter and resolution limit. (A) Because light has wave properties, a point emitter interferes as a bright circle with dark and bright concentric rings around it on the image plane. (B) The resolution of a microscope is the smallest distinguishable distance between two partially overlapping PSFs. In the left image, the two objects can be distinguished, because $d = d_{lim}$ but in the right image $d < d_{lim}$ and therefore cannot be resolved.

To maximize the resolving power of a microscope, a proper choice of the pixel size is essential. According to the Nyquist-Shannon sampling theorem, the pixel size for an image with a resolution of for example 250 nm needs to be smaller than 125 nm, since for an accurate digital representation, the signal should be oversampled by the factor of two at minimum [5].

With the discovery of fluorescence and the invention of fluorescence microscopy, the contrast of the images was significantly improved by attaching fluorescent molecules to structures of interest and hereby making it easier to distinguish between the region of interest, background and scattered light [5].

The fluorescence effect is mediated by certain molecules and minerals. Organic dyes (e.g., the Alexa dyes) have the advantage of being stable and bright, whereas fluorescent proteins (e.g., green fluorescent protein (GFP)) can be expressed by the cell itself. Both can emit light upon the absorption of photons because the energy of this photon can lead into an excited electronic state of the fluorescent molecule, which can switch back to the ground state by emitting a photon. The wavelength of the

emitted photon matches the energy difference between ground and excited electronic state and is longer, thus shifted more to the red color range, compared to the corresponding excitation photons (**Figure 4**). This so called 'Stokes shift' occurs because the molecules loose energy in the excited electronic state due to non-radiative processes as for example molecular vibrations, what - according to Planck's law - results in longer wavelength in the emission light [5].

A fluorescent molecules lifetime is not unlimited and depends on different factors. For example, the number of emission cycles, the excitation intensity and the contact to molecular oxygen lead to a permanent loss of fluorescent intensity, called bleaching [25].

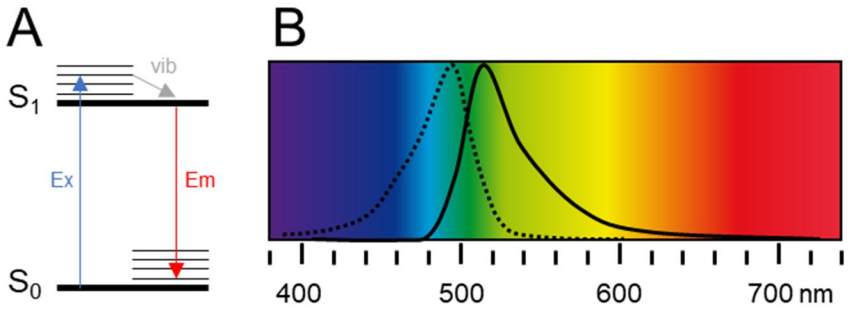

Figure 4: Jablonski diagram of a single molecule emitter and excitation and emission spectrum of the organic dye Alexa 488. (A) The ground and excited electronic state energy bands (S_0 & S_1) of a single molecule emitter span a series of vibrational levels. After excitation (Ex), non-radiative processes, as for example molecular vibrations (vib), result in energy loss and an emitted photon with lower energy and longer wavelength (Em). (B) The organic dye Alexa 488 has an excitation maximum of 490 nm (dotted line) and a red shifted emission maximum of 525 nm (solid line).

1.2.2 Types of microscopes

In the following section, a selection of types of microscopes will be explained.

Widefield microscopy

In widefield microscopy, the whole sample is illuminated. The widely used epifluorescent microscopes use the same lens as condenser and objective. Through this setup, most of the excitation light passes through the sample without being absorbed and never reaches the detector (**Figure 5.A**) The light emitted by the sample is separated from the backscattered excitation light by a dichroic mirror and an emission filter, before being processed by a camera [5].

Confocal microscopy

In confocal microscopy, only a very small volume of the sample is illuminated by focusing the light on a small spot, the confocal volume. Emitted light is collected by the objective lens and projected onto a light sensitive point detector. To observe the whole sample, the illumination volume is moved by a set of movable mirrors over the whole sample, while a computer digitally reconstructs an image out of the information collected by the detector (**Figure 5.B**). The use of a pinhole in front of the detector (**Figure 5.C**) eliminates out-of-focus light, which is not originating from the focal layer, improves signal-to-noise ratio and contrast and brings the possibility to image 3D samples (due to the improved axial resolution) [5].

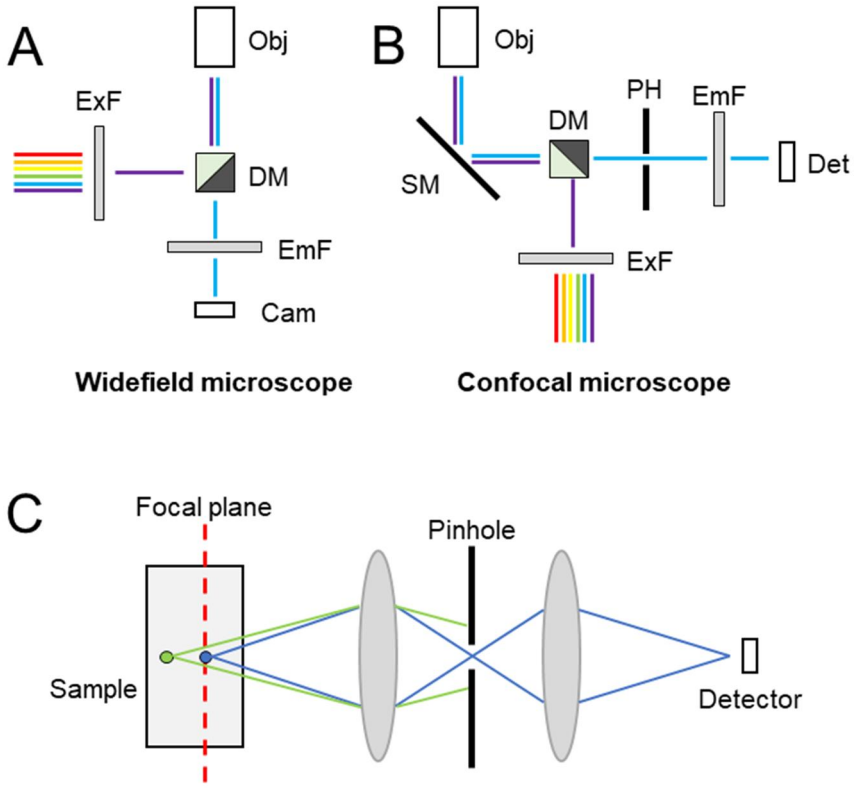

Figure 5: Differences between widefield microscopes and confocal microscopes. (A) In a widefield microscope, excitation and emission follow the same path to and from the objective (Obj). The excitation light illuminates the whole sample and is separated from the emitted light by the dichroic mirror (DM). Additionally, excitation and emitted light are filtered by excitation (ExF) and emission (EmF) filters, before being recorded by a camera (Cam). (B) In confocal microscopy, the light is focused on a small volume and moved by a scanning mirror (SM) to observe the whole sample. The pinhole (PH) eliminates out-of-focus light and especially improves the resolution in z-direction. Images are acquired using light sensitive point detectors. (C) The pinhole in a confocal microscope is responsible for the elimination of out-of-focus light and thus provides axial sectioning.

Super-resolution microscopy

Over the years, scientists developed methods to push the resolution of the microscopes further than it was possible with standard confocal or widefield microscopes. With so called ‘super-resolution microscopy’, it is possible to overcome the physical limitations regarding the spatial resolution of light microscopy and image subcellular structures and processes which remained elusive before.

One way to bring the resolution of a microscope beyond the Abbe limit is ‘Re-scan confocal microscopy’ (RCM). A RCM microscope is based on a conventional confocal setup with an attached Re-scan unit, whose most important part is a second scanning mirror, ‘writing’ the passing light directly onto a camera and producing a magnified image (**Figure 6**). The advantage of a RCM is the ‘optics-only’ super-resolution method and in contrast to ‘Structured Illumination Microscopy’ (SIM), no image reconstruction is needed after acquisition. The lateral resolution is improved by the factor $\sqrt{2}$ to around 170 nm compared to confocal microscopy. Furthermore, sensitivity is strongly improved due to a relatively wide-open pinhole [26].

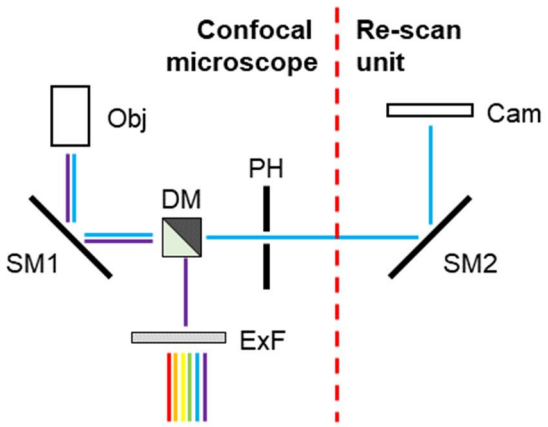

Figure 6: Setup of a Re-scan confocal microscope (RCM). The first unit of the RCM is a conventional confocal setup with excitation filter (ExF), dichroic mirror (DM), scanning mirror (SM1), objective (Obj) and a pinhole (PH). The image is scanned by SM1 and projected through the PH. Here, the re-scan unit is attached, mainly consisting out of a second scanning mirror (SM2) and a camera (Cam). The light passing the PH is re-scanned by SM2 onto Cam, producing a magnified image.

In SIM, the sample is illuminated with a periodic, structured pattern, resulting in Moiré images (**Figure 7**), which can be computationally reconstructed to a high resolved image. The possible lateral resolution improvement towards confocal microscopy is limited by the factor 2, means to around 125 nm. SIM has the disadvantage that samples are long exposed to high illumination intensities.

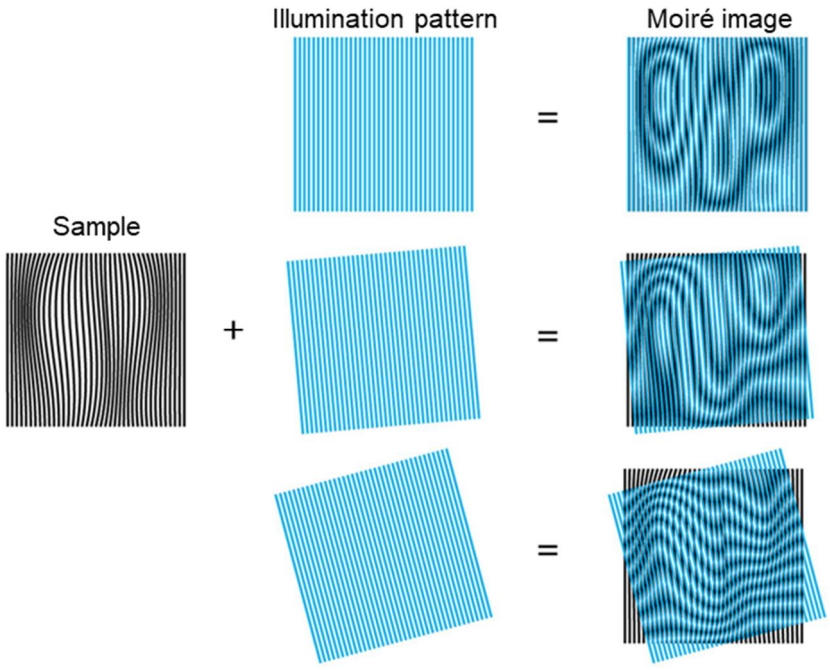

Figure 7: Imaging process in 'Structured Illumination Microscopy' (SIM). The sample is illuminated with a structured pattern, whose resulting images are reconstructed by a computer. Adapted from Vangindertael et al. [5])

Some super-resolution techniques can even reach resolutions in the range of nanometers. Fluorophores located closer than the diffraction limit can be made resolvable by imaging them separately (**Figure 8**).

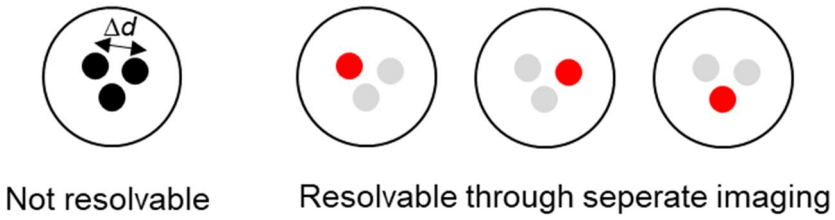

Figure 8: Resolution increase through separate imaging. When the distance *d* between two fluorophores is smaller than the diffraction limit, they cannot be resolved with conventional light microscopy. When the fluorophores emit at separate timepoints, they can be resolved even when they are closer than the diffraction limit.

The technique 'stochastic optical reconstruction microscopy' (STORM) selectively switches on only a fraction of the fluorophores in a sample. Imaging is performed over many cycles by subsequent localization of the emitter events. The switching in STORM is induced by a reducing buffer environment [7], whereas in 'photoactivated localization microscopy' (PALM), which follows the same principle, switching is induced by short-

wavelength excitation [27]. Lateral resolutions below 20 nm and axial resolutions of 50 nm can be reached with this techniques [28].

‘Stimulated emission depletion microscopy’ (STED) reaches high resolutions by selectively and reversibly switching off fluorophores close to the excitation volume through a STED-laser with red-shifted wavelength and hereby reducing the illumination PSF size [29].

1.2.3 Labeling strategies and chromatic aberration

The advantage of fluorescence microscopy is that structures can be labeled specifically to visualize their exact position and/or movements. Fluorescence microscopy offers the researcher a big choice of different labels. Fluorescent proteins, as for example green fluorescent protein (GFP) have the big advantage being expressed by cells itself and do not need to get introduced from outside. Coupled to a protein of interest, it allows temporal and spatial imaging of this protein [30]. Organic dyes as the Alexa and Atto species need a linker to be coupled to the region of interest but are brighter and more stable. Fluorophore coupled antibodies can bind covalently to a structure of interest (epitope) and thereby attaching the fluorophore at the correct position. With the advent of super-resolution techniques and increasing achievable resolutions in fluorescent microscopy, locating the fluorophore as close as possible to the epitope became more and more necessary [31].

Depending on the resolution of the setup, the quality and accuracy of the image suffers, when the sample is labeled with standard IgG antibodies. IgG antibodies translocate the fluorophore around 10 nm from the original epitope, what can be a lot, especially when a primary and a secondary antibody are used [32]. To minimize this so called ‘linkage error’, new labelling strategies needed to be introduced. Based on the classical IgG antibody, there are several ways to reduce the linkage error. An IgG antibody consists out of different variable as well as constant protein chains and is divided into two regions (**Figure 9**). The F_{ab} region exists twice and contains the antigen-binding sites, whereas the F_c-region exists once and is more involved in information transfer than in antigen binding. By splitting the antibody using the enzyme Papain, two separate F_{ab}-fragments can be extracted, reducing the linkage error due to the smaller total size. This size can be reduced further when nanobodies are used, which only consist out of the variable antigen binding domains. Both, F_{ab}-fragments and

nanobodies show sufficient antigen affinity for antigen binding and can be coupled to fluorescent molecules [33].

Depending on the requirements for a label, also different customized solutions can be manufactured. For example, the use of trifunctional labels allows the combination of an antibody with two different functional domains, for example a fluorophore or a crosslinker (**Figure 10**) [8]. Besides antibodies, it is also possible to use fluorescent labeled peptides like Phalloidin to stain certain structures, like in this thesis F-actin [34]. This labeling technique was used in the experiments described below, besides fluorescent labeled antibodies and F_{ab}-fragments.

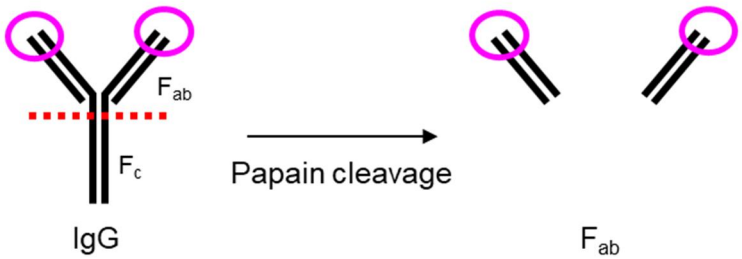

Figure 9: Fab-Fragment production through IgG antibody cleavage. The IgG antibody consists out of two F_{ab}-regions and one F_c region. Using the enzyme papain, the antibody is dissected, and two single F_{ab}-fragments can be extracted with the same antigen-binding sites (marked in magenta).

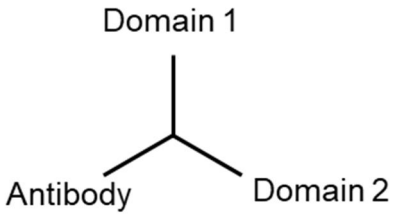

Figure 10:Trifunctional label. The antibody can be extended with two different functional domains.

Chromatic aberration

Especially when imaging in the super-resolution range, extra care needs to be taken when imaging samples with different fluorophores, since the refractive index of a lens varies with changing wavelengths, leading to slightly shifted channels between different fluorophores. Although in well corrected systems, these shifts are extremely small, they can be big enough to affect the results of colocalization analysis [5]. To correct this effect, computational correction masks can be generated (as described in 2.2.6.2.1), using multiple images of beads, acquired using the respective excitation wavelengths for the specific sample.

1.2.4 Expansion microscopy

In the year 2015, the laboratory of Edward Boyden developed a completely new approach to push the resolution of a microscope to the super-resolution level. The technique he first described is known as 'Expansion Microscopy' and uses the help of a swellable hydrogel to physically expand the sample, thereby increasing the effective resolution (both in lateral and axial direction), while the true resolution of the microscope is not in super-resolution range. Therefore, the big advantage of this method is, that super-resolution can be reached using a standard confocal or widefield microscope [8].

1.2.4.1 Principle of Expansion Microscopy

The concept of ExM as described by the Boyden group [8] is based on the six steps drawn out in **Figure 11**. To optimize the protocol and to adapt it for different sample textures and labeling strategies several modified protocols have been developed by different groups. In the following, the single steps (Fixation, Labeling, Linking, Gelation, Digestion, Expansion, Imaging) and their modifications are described.

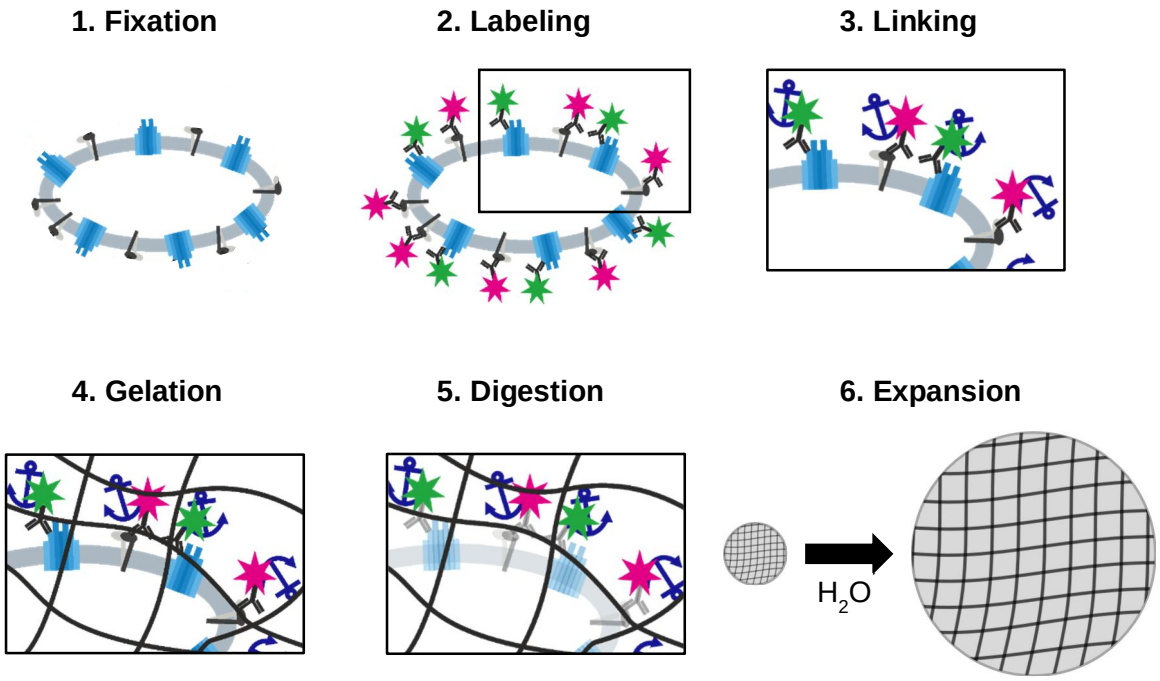

Figure 11: Principle of Expansion microscopy: Schematic illustration of the important steps in Expansion microscopy. Kindly provided by Hannah Heil.

1. *Fixation:* The first step in the ExM protocol is the fixation of the samples, where the standard fixative paraformaldehyde (PFA) can be used as demonstrated by

the Boyden group in their pioneering article [8]. In 2017, the laboratory of S. Rizzoli introduced Glyoxal as a general alternative to PFA with faster and stronger fixation properties and - more important - brighter images, probably due to more available epitopes for the antibodies after fixation [35]. Truckenbrodt and co-authors first integrated Glyoxal in an ExM protocol [36].

2. *Labeling:* To visualize the structure of interest during imaging, the sample needs to be labeled. The first ExM approach by the Boyden group [8] used a trifunctional label which contained one domain with a complementary oligonucleotide strand, one with a fluorophore and one with a methacryloyl group, which is later linked into the growing monomer gel matrix. By examining the use of different fluorescent-labeled antibodies and fluorescent proteins in ExM, the Boyden group amplified the choice of labels and showed their varying applicability [37]. Because the production of the trifunctional labels as mentioned above is complicated and time-consuming, the use of conventional fluorescent-labeled antibodies and fluorescent proteins is more common. A different labeling strategy was introduced by Tillberg et al., who established labeling after the digestion step and thereby reducing fluorophore loss during sample preparation (mostly during digestion). [37].
3. *Linking:* In the next step the sample and fluorophores need to be supplied with a reactive unit, which links into the hydrogel during the gelation process. When trifunctional labels are used, this is achieved through the contained free acrylamide end, whereas when fluorescent-labeled antibodies are used, linking is facilitated by linking substances like Glutaraldehyde [8], [38] and recently Acryloyl-X (AcX), which preserves the fluorescence intensity better and produces less unspecific background signal [37].
4. *Gelation:* After preparing the sample with the linker, it is embedded in a gel consisting out of acrylamide and the cross-linker N,N′-methylenebisacrylamide. Their exact ratio in the gel determines the expansion factor and is a tradeoff between gel stability and expansion factor. Free radical polymerization is initiated by ammonium persulfate (APS) and accelerated by tetramethylethylenediamine (TEMED) [8]. During the polymerization, the acrylamide ends of the linker are integrated and become strongly connected to the gel matrix.

5. *Digestion:* To allow isotropic expansion of the gel when immersed into water, the sample needs to be digested to destroy all internal bonds and thereby eliminate intracellular resistances. Depending on the probe properties and the protocol, different enzymes or detergents like Proteinase K [8], LysC [37] or SDS [39] can be used for digestion/denaturation.
6. *Expansion:* As a last step, the gel is washed and bathed several times in fresh deionized water to reach the maximal possible expansion factor (around 4 or 10 times depending on the protocol).

Eventually, the gel is largely watery 'empty' but keeps the fluorophores in place that still mark the original position of the biomolecules to be visualized. The large proportion of water makes the sample transparent and homogenous concerning the refractive index, and thus ideally suited for large volume 3D imaging, since the expansion takes place isotropically. The gels can then be imaged, using a standard confocal or widefield microscope, even combinations with other super-resolution techniques are possible.

1.2.4.2 Different approaches to the ExM protocol and combination with super resolution techniques

After the introduction of ExM by the Boyden group [8], which reached a lateral resolution of around 70 nm, many new approaches were developed, variating the composition of the gel and/or the sequence of the single protocol steps. Chang and co-authors [40] pushed the resolution through iterative ExM up to 25 nm. Truckenbrodt and co-authors [41] reached the same resolution by changing the components of the gel (10xExM). Experimental studies of Tillberg and co-authors [37] and Gambarotto and co-authors (Ultrastrucure-ExM, U-ExM) [39] were able to reduce the loss of fluorescent signal due to the exposition of the fluorophore to digestion reagents by introducing a protocol, allowing post-denaturation staining.

Depending on the application, the resolution achieved by ExM may not be sufficient. Therefore, there are several approaches for the combination of ExM with super-resolution techniques. Gao and co-authors [42] showed that the combination of ExM and STED (ExSTED) can reach a lateral resolution of <10 nm. Wang and co-authors [43] combined ExM with SIM (SIM-ExM) and achieved lateral resolution of 30 nm. These approaches mainly improve the lateral resolution but not the axial resolution. Axial and lateral resolution improvement resulting in 35 nm isotropic resolution were reported by Tong and co-authors [44] by a combination of ExM with STORM that even allows multicolor imaging. Unfortunately, the labeling strategy and limited choice of

fluorophores may require large preparatory and experimental efforts and compromises.

1.3 Colocalization analysis as a method to quantify interactions between different structures

The localization, distribution and interaction of proteins play a crucial role in the understanding of biological processes. Simple visualization often does not result in sufficient comprehension. Colocalization analysis is a computer-assisted approach to quantify the spatial overlap between two different fluorescent labels and thus the interaction of two molecular species. For the correct interpretation of colocalization results, the spatial resolution of the image data needs to be taken into account, since non-resolved interaction partners in the image result in false-positive results as by definition nearest neighbors overlap in an insufficiently resolved image. Especially the axial resolution, which is weaker as the lateral one need to be taken into account as otherwise elements may appear colocalized which are rather stacked on top of each other with gaps than sharing an ‘interaction zone’.

The most basic approach to quantify colocalization is based on the Pearson correlation coefficient (PCC) (**Figure 12**). This coefficient ranges from 0 (no colocalization) to 1 (full colocalization) and depends on the number of colocalized pixels but also takes the mean intensity of a channel into account. There are several other coefficients, as for example the Manders’ coefficient, which is almost independent of signal proportionality because it does not consider the channels mean intensity and is therefore more sensitive to background signal [45] [46].

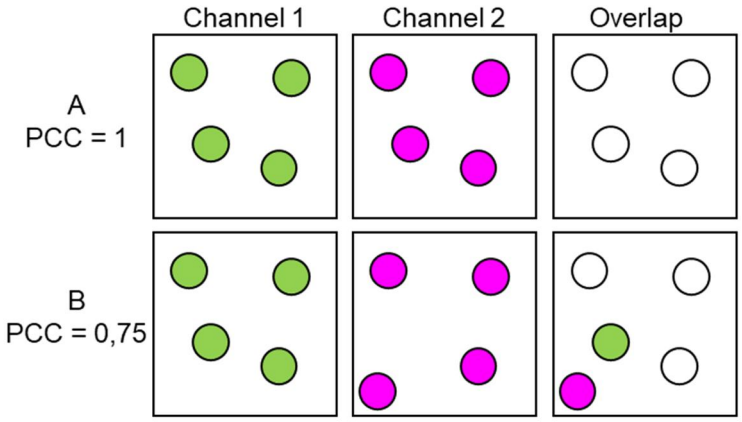

Figure 12: Determination of the *Pearson correlation coefficient* (PCC). The PCC takes values from 0 (no colocalization) to 1 (full colocalization).

1.4 Aim of this study

The aim of this study was to establish an optimized protocol for ExM with murine blood platelets followed by dual-color 3D imaging with optimized imaging settings and colocalization based image analysis to map membrane receptor distributions and interactions. This approach will provide a toolset for the investigation of membrane receptor distribution in fixed platelets, like receptor dimerization and reorganization upon activation and receptor interaction with intracellular components like the cytoskeleton. This toolset will help to visualize and understand so far not depictable interactions and (co-) localizations, which leads to a better understanding of receptor distribution and localization on and in the platelet.

In a first step, the protocol of the first ExM approach by Boyden, which was developed for cultured cells and brain tissue, needed to be adjusted for platelets. These modifications were necessary to meet the requirements of platelets and to maximize the final fluorescent intensity of the sample, and therefore minimize the fluorophore loss during the specimen preparation protocol. Since different antibody/fluorophore combinations showed variable compatibility with the ExM protocol and sometimes resulted in very dim samples, a library of compatible antibodies needed to be set up, so that suitable antibodies can be found fast and reliably. Furthermore, to realize the investigation of the interaction of platelet membrane receptors and components of the cytoskeleton, an ExM protocol including the simultaneous staining of intra- and extracellular components were developed.

Besides the optimization of the ExM protocol itself, an image acquisition and an image analysis pipeline were developed to evaluate and validate the approach of mapping platelet receptor distributions based on the colocalization analysis of multicolor 3D ExM images.

Finally, as the field of ExM is rapidly developing, new protocol approaches were tested, as well as the combination of ExM with other super-resolution methods.

2 Materials and Methods

2.1 Materials

2.1.1 Chemicals and reagents

Chemical/reagent	Company
Acrylamide	Sigma (Steinheim, Germany)
2-(N-Morpholino)-ethansulfonsäure (MES)	Sigma-Aldrich (Steinheim, Germany)
4-(2-hydroxyethyl)-1-piperazineethanesulfonic acid (HEPES)	Roth (Karlsruhe, Germany)
Acryloyl-X, SE	invitrogen (Germany)
Ammonium persulphate (APS)	Roth (Karlsruhe, Germany)
Apyrase	Sigma-Aldrich (Schnelldorf, Germany)
Ascorbic Acid	Roth (Karlsruhe, Germany)
Bovine serum Albumin (BSA)	Roth (Karlsruhe, Germany)
Calcium chloride (CaCl2)	Roth (Karlsruhe, Germany)
Catalase	Sigma (Steinheim, Germany)
Chloroform	Sigma-Aldrich (Steinheim, Germany)
Dulbeccos Modified Eagle Media (DMEM)/F12	Gibco (Karlsruhe, Germany)
Ethanol	Sigma-Aldrich (Steinheim, Germany)
Ethylene glycol-bis(β-aminoethyl ether)N,N,N',N'-tetraacetic acid (EGTA)	Sigma-Aldrich (Steinheim, Germany)
Ethylenediaminetetraacetic acid (EDTA)	AppliChem (Darmstadt, Germany)
Fluoroshield™	Sigma-Aldrich (Steinheim, Germany)
Glucose	Sigma-Aldrich (Steinheim, Germany)
Glucose-oxidase	Roth (Karlsruhe, Germany)
Glutaraldehyde	Sigma-Aldrich (Buchs, Switzerland)
Glycine	AppliChem (Darmstadt, Germany)
Glyoxal	Sigma-Aldrich (Schnelldorf, Germany)
Guanidine-HCl	Sigma (Steinheim, Germany)
Heparin	Sigma-Aldrich (Schnelldorf, Germany)
Magnesium Chloride (MgCl2)	AppliChem (Darmstadt, Germany)
N,N′-Methylenebisacrylamide	Sigma (Steinheim, Germany)
N,N-dimethylacrylamide (DMAA)	Sigma-Aldrich (Steinheim, Germany)
Pen Strep (Penicillin Streptomycin)	Gibco, Life Technologies (Darmstadt, Germany)
Phosphate Buffer Saline (PBS)	Life Technologies (Darmstadt, Germany)
Poly- D Lysine	MP Biomedicals (Santa Ana, United States)
Potassium Chloride (KCl)	Roth (Karlsruhe, Germany)
Prostacyclin (PGI2)	Sigma-Aldrich (Schnelldorf, Germany)
Proteinase K, recombinant, PCR	ThermoScientific (Lithuania)
Sodium acrylate	Sigma-Aldrich (Steinheim, Germany)

Chemical/reagent	Company
Sodium bicarbonate (NaHCO3)	Sigma (Steinheim, Germany)
Sodium Chloride (NaCl)	Roth (Karlsruhe, Germany)
Sodium dihydrogen phosphate (NaH2PO4)	Roth (Karlsruhe, Germany)
Sodium Hydroxide (NaOH)	Roth (Karlsruhe, Germany)
Tetramethylethylenediamin (TEMED)	Roth (Karlsruhe, Germany)
Tris (hydroxymethyl) aminomethane, pH 8	AppliChem (Darmstadt, Germany)
Trition X100	Roth (Karlsruhe, Germany)
Trypsin	PAN, Biotech (Germany)
Tween-20	Roth (Karlsruhe, Germany)
Thrombin	Roche Diagnostics (Mannheim, Germany)

2.1.2 Materials

Material	Vendor
Round Glass Coverslip (12mm and 24 mm Diameter)	Marienfeld (Germany)
Heparinized capillaries	Hartenstein (Würzburg, Germany)
Syringe	Primo (Poland)
Syringe Filter (0.45µm)	Sartorius (Göttingen, Germany)
Well plate (6 well)	ThermoScientific (Roskilde, Denmark)
Petridish	ThermoScientific (Roskilde, Denmark)
Parafilm (stretchable semi-transparent foil)	Pechiney (Chicago, IL, USA)
Heating mat	TRIXIE Heimtierbedarf, (Tarp, Germany)
Microscope slides	ThermoScientific (Roskilde, Denmark)

2.1.3 Antibodies

Antibody	Clone	Isotype	Antigen	Fluoro-phore	F_{ab}-Frag-ment	Company/ description
p0p/B	57E12	IgG2b	GPIbα	Alexa Fluor 488	yes	[47]*
p0p/B	57E12	IgG2b	GPIbα	FITC	no	[47]*
p0p4	15E2	IgG2b	GPIbα	Alexa Fluor 488	yes	[20]*
p0p4	15E2	IgG2b	GPIbα	Alexa Fluor 488	no	[20]*
p0p4	15E2	IgG2b	GPIbα	Atto 647N	yes	[20]*
p0p4	15E2	IgG2b	GPIbα	FITC	no	[20]*
p0p/A	92H12	unknown	GPIbα	Alexa Fluor 488	no	Unpublished
p0p/A	92H12	unknown	GPIbα	Alexa Fluor 546	no	Unpublished
p0p/A	92H12	unknown	GPIbα	FITC	no	Unpublished
p0p1	3G6	IgG1	GPIbβ	Alexa Fluor 488	no	[20]*
p0p1	3G6	IgG1	GPIbβ	Alexa Fluor 594	no	[20]*
p0p1	3G6	IgG1	GPIbβ	FITC	no	[20]*
p0p3	7A9	IgG2a	GPIbα	FITC	no	[20]*
MWReg30	5D7	IgG1	GPIIb/IIIa	Atto 647N	no	[20]*
MWReg30	5D7	IgG1	GPIIb/IIIa	Alexa Fluor 488	no	[20]*
MWReg30	5D7	IgG1	GPIIb/IIIa	Alexa Fluor 532	yes	[20]*
MWReg30	5D7	IgG1	GPIIb/IIIa	FITC	no	[20]*
JON6	14A3	IgG2b	GPIIb/IIIa	Alexa Fluor 546	no	Unpublished
JON6	14A3	IgG2b	GPIIb/IIIa	Alexa Fluor 488	no	Unpublished
JON6	14A3	IgG2b	GPIIb/IIIa	FITC	no	Unpublished
JON/A	4H5	IgG2b	GPIIb/IIIa	FITC	No	[48]*
JON2	45A9	IgG2a	GPIIb/IIIa	FITC	No	[20]*
EDL1	57B10	IgG2a	GPIIIa	FITC	No	[20]
p0p6	56F8	IgG2b	GPIX	Atto 647N	No	[47]*
p0p6	56F8	IgG2b	GPIX	Alexa Fluor 594	No	[47]*
p0p6	56F8	IgG2b	GPIX	Alexa Fluor 488	No	[47]*
p0p6	56F8	IgG2b	GPIX	FITC	No	[47]*

* Labeled in house

F_{ab} fragments were produced in house out of the corresponding IgG antibody.

Commercial Antibodies

Antibody	**Company/description**
Monoclonal Anti β tubulin (mouse)	Sigma (Steinheim, Germany)
Goat anti-mouse IgG (H+L)-Alexa 532	Thermo Fisher Scientific (Rockford, USA)
Goat anti-mouse IgG (H+L)-Alexa 594	Labeled in house
Anti-tubulin Alexa 488	Life Technologies (Darmstadt, Germany)
WGA-Alexa 647	Thermo Fisher Scientific (Rockford, USA)
Alexa Fluor 647	Thermo Fisher Scientific (Rockford, USA)
Hoechst 405	Sigma-Aldrich (Steinheim, Germany)
TetraSpeck™ Microspheres, 0.2 µm, fluorescent blue/green/orange/dark red	Invitrogen
Actin ExM	Chrometra (Kortenaken, Belgium)
Monoclonal Anti-β-Actin antibody produced in mouse	Sigma-Aldrich (Steinheim, Germany)

2.1.4 Buffers and stock solutions

Blocking buffer

5% BSA in 1x PBS

Cytoskeleton Buffer (CS-Buffer)

MES	10 mM
NaCl	150 mM
EGTA	5 mM
Glucose	5mM
$MgCl_2$	5mM
pH: 6.1	

Cytoskeleton Buffer 1 (CS-Buffer 1)

Glutaraldehyde (v/v)	0.3 %
Triton X-100	0.25 %
In CS-Buffer	

Cytoskeleton Buffer 2 (CS-Buffer 2)

Glutaraldehyde (v/v)	2 %
In CS-Buffer	

Denaturation Buffer (for U-ExM protocol)

SDS	200 mM
NaCl	200 mM
Tris	50 mM

Digestion Buffer (for 4x- and 10xExM protocol

Tris pH 8.0	50 mM
EDTA pH 8.0	1 mM
Guanidine HCl	0.8 M
Triton X-100 (v/v)	0.5 %
Added shortly before use	
Proteinase K	8 Unit/mL

Glyoxal Buffer

Ethanol (v/v)	19.9 %
Glyoxal (v/v)	7.9 %
Acetic acid	0.76 %
pH was adjusted with NaOH to	5

Monomer Solution (4xExM protocol)

Sodium acrylate (w/v)	8.6 %
Acrylamide (w/v)	2.5 %
N,N′-Methylenebisacrylamide (w/v)	0.15 %
Sodium chloride	2 M
PBS	1x
Added shortly before gelation:	
TEMED (v/v)	0.2 %
APS (w/v)	0.2 %

Monomer Solution (10xExM protocol)

DMAA (w/w)	2.67 %
Sodium Acrylate (w/w)	0.64 %
Added shortly before gelation:	
TEMED (v/v)	0.004 %
KPS	0.4 M

Monomer Solution (U-ExM protocol)

Sodium acrylate (w/w)	19 %
Acrylamide (w/w)	10%
N,N′-Methylenebisacrylamide (w/w)	0.1 %
PBS	70.9 %
Added shortly before gelation:	
APS (w/v)	0.5 %
TEMED	0.5 %

Phosphate Buffered Saline (PBS)

NaCl	137 mM
KCl	2.7 mM
KH_2PO_4	1.5 mM
Na_2HPO_4	8 mM

PLP (Periodate-lysine-paraformaldehyde)

Lysin (w/v)	1.35 %
$NaHPO_4$	9.38 mM
NaH_2PO_4	28.13 mM
PFA	3 %
$NaIO_4$ (w/v)	0.25 %

Tyrode’s Buffer

NaCl	137 mM
Na_2HPO_4	0.43 mM
KCl	2.7 mM
$NaHCO_3$	12 mM
HEPES	5 mM
$MgCl_2$	1 mM
BSA (v/v)	0.35 %
Glucose (v/v)	0.1 %

Tyrode's Buffer with Calcium

NaCl	137 mM
Na2HPO4	0.43 mM
KCl	2.7 mM
NaHCO3	12 mM
HEPES	5 mM
MgCl2	1 mM
CaCl2	2 mM
BSA (v/v)	0.35 %
Glucose (v/v)	0.1 %

Washing Buffer

0.1% Tween-20 in PBS 1x

All buffers were prepared and diluted in deionized water obtained from a water purifier from TKA/Millipore.

2.2 Methods

2.2.1 Coverslip cleaning

Every glass coverslip used in the experiments was cleaned according to the following protocol: Coverslips (12- or 24-mm diameter) were placed in racks and sonicated for 1 h in Chloroform. The racks were taken out of the Chloroform bath and after drying for a few minutes, sonicated again for 1 h in 5M NaOH. Afterwards the coverslips were washed 3 times in double-distilled water (ddH_2O). For drying, the coverslips were placed in a UNB 100 oven (Memmert, Schwabach, Germany) at 60°C for 2-3 h. The coverslips were stored in Ethanol until used.

2.2.2 Coverslip coating

2.2.2.1 Glycine coating

Cleaned coverslips were coated with 2 M glycine in PBS for 10 min at RT. After washing twice with PBS and one time with Tyrodes, coverslips were air-dried.

2.2.2.2 Fibrinogen coating

Cleaned coverslips were coated with 0.1 % Fibrinogen in PBS (v/v) overnight at 4 °C. Next, they were blocked for at least one hour with 1 % BSA in PBS (w/v).

2.2.2.3 Poly-D-Lysine coating

Cleaned coverslips were coated with 0.25 mg/ml Poly-D-Lysine for 10 min at RT. Coverslips were gently washed with excess of ddH_2O and dried with N_2.

2.2.3 Sample Preparation

2.2.3.1 CHO cells

Cell culture

CHO cells were cultured in DMEM/F12 with 10 % FCS and 1 % Pen/Strep.

Seeding

CHO cells from the cell culture were counted in a Neubauer chamber. Cleaned coverslips (12 mm for expanded samples, 24 mm for not-expanded control samples) were placed in six-well-plates and 2 ml DMEM/F-12 with 10 % FCS and 1 % Pen/Strep including 200,000 cells were added. CHO cells were incubated at 37 °C and 5 % CO_2 overnight.

Fixation

The growth media was discarded from the six-well-plates and the coverslips were transferred onto a flat surface (e.g., cover of a six-well-plate) coated with an stretchable semi-transparent foil (Parafilm, Pechiney, Chicago, IL, USA). Prewarmed CS-Buffer 1 was added on the coverslip for 2 min, then CS-Buffer 2 was added for another 10 min at 37 °C.

Blocking and Immunolabeling

Cells were blocked with Blocking Buffer for 30 min. Afterwards cells were incubated for 60 min at RT with 10 µg/ml of primary antibody diluted in Blocking Buffer. Samples were washed twice with 1 % TWEEN-20 and twice with PBS, for 5 min respectively at RT. Next, samples were incubated for 60 min at RT with 10 µg/ml of primary antibody diluted in Blocking Buffer. Again, coverslips were washed with 0.1 %TWEEN-20 for 1 min and twice for 2 min. Last, they were washed twice with PBS for 5 min, respectively.

2.2.3.2 Blood platelets

Platelet purification

The blood platelets were separated from the other components of the blood by differential centrifugation. Mice were anesthetized in an isoflurane-chamber. Around 700 µl blood were withdrawn from the retroorbital plexus and collected in Eppendorf tubes containing 300 µl heparin (20 U/ml). Samples were centrifuged at 800 rpm for 6 min in an Eppendorf Centrifuge 5415C. The upper phase plus some erythrocytes were transferred into a new tube containing 300 µl heparin. The same cycle of

centrifugation (6 min at 800 rpm) was performed. Only the upper phase (platelet rich plasma, PRP) without any erythrocytes was transferred into a new tube. The samples were centrifuged in an Eppendorf Centrifuge 5424 for 5 min at 2,800 rpm. The supernatant was discarded, and the pellet resuspended in 1 ml of prewarmed (37 °C) Tyrode's buffer without Calcium plus apyrase and PGI_2 (final concentration: 0.02 U/ml and 50 mM respectively). Samples were again centrifuged for 5 min at 2,800 rpm. Supernatant was discarded and pellet resuspended, as described in the step before. For platelet count measurement 50 µl platelet suspension was mixed with 50 µl PBS and analyzed, using a Sysmex KX-21N automated hematology analyzer (Sysmex Corporation, Kobe, Japan). Samples with MPV (Mean Platelet Volume) > 6 were discarded, because this is a sign for platelet activation. Platelet concentration was adjusted to 300,000 platelets per µl, by diluting the pellet with the appropriate amount of Tyrode's buffer without Calcium, containing 0.02 U/ml apyrase). Next, the platelets were set to rest for 30 min at 37 °C.

Platelet activation

This step was only performed if the experiment required the platelets to be activated. After 30 min resting time, platelets were diluted to 100,000 platelets per µl in Tyrode's buffer with Calcium. For platelet activation 0.01 U/ml Thrombin was added to the platelet suspension. Subsequently, the activated platelets were left for spreading as described below. Platelet were only activated for the experiments described in 3.1.5.3 and 3.1.4.

Platelet spreading and fixation

Non-activated platelets were diluted to 150,000 platelets per µl. (Activated platelets: 100,000/µl). The platelet suspension was added for spreading on glycine coated coverslips (activated platelets: fibrinogen coated coverslips). For samples that were used for expansion, 110 µl platelet suspension were applied to coverslips with a diameter of 12 mm. For control samples that were not expanded, 220 µl of platelet suspension and coverslips with a diameter of 24 mm were used. Not activated platelets were left for spreading for 20 min at 37 °C, in case of activated platelets, spreading time was decreased to 15 min to get platelets in different stages of spreading. After spreading, coverslips were washed twice with Tyrode's buffer and fixed as described below.

Fixation

Protocol differed depending on the fixative used:

(a) PFA: 4 % PFA was applied for 20 min at 37 °C.

(b) Glyoxal: Glyoxal buffer was applied for 20 min at 37 °C in the beginning of the project, later only for 10 min.

(c) CS-Buffer: CS-Buffer 1 was applied for 2 min at 37 °C. CS-Buffer 2 was applied afterwards for 10 min at 37 °C.

(d) PLP: PLP was applied for 20 min at 37 °C

Fixed samples were washed 5 times with PBS for 30 s, 1 min, 5 min, 10 min, and 15 min, respectively. Afterwards, samples were blocked and labeled before either expanding or preserving them (see Preservation of unexpanded control samples below).

Blocking and Immunolabeling (except for Actin-ExM/Phalloidin)

Samples were blocked with 5 % BSA in PBS for 2 h at RT and afterwards incubated with the antibody (10 µg/ml in 5 % BSA in PBS) for 30 min at 37 °C. Samples were washed 5 times with PBS for 30 s, 1 min, 5 min, 10 min, and 15 min respectively. Subsequently, samples planed for expansion continued with the Expansion protocol (2.2.4), whereas control samples which remained unexpanded were preserved (see Preservation of unexpanded control samples below).

Blocking and Immunolabeling (Actin-ExM/Phalloidin)

Samples were blocked in 5.34 % BSA, 0.01 % Tween-20, 1.16 % Acryloyl-X and 2.5 % Actin ExM in PBS for 30 min at 37 °C. Samples were washed twice with PBS. Subsequently, samples planed for expansion continued with the Expansion protocol (2.2.4), whereas control samples which remained unexpanded were preserved (see Preservation of unexpanded control samples below).

Preservation of unexpanded control samples

Unexpanded control samples were treated with Fluoroshield and fixed with nail enamel on rectangular glass slides (24 x 50 mm).

2.2.4 Expansion Protocol

Three different expansion protocols were used and optimized. 4x and 10xExM mainly differentiates by the monomer solution used, while UltraExM uses a different labeling strategy (post-gelation labelling). The 4x ExM protocol is based on the master thesis work of Shazeb Ahmad performed also in the AG Heinze, RVZ, Würzburg, Germany [49].

2.2.4.1 ExM with expansion factor 4 (4xExM)

Anchoring

After immunolabeling of the samples, they were treated with Acryloyl-X, SE (0.1 mg/ml in PBS).

Gelation

Surface preparation: To obtain a flat surface for gelation, the cover of a six-well-plate was covered with stretchable semi-transparent foil. Gelation solution was prepared on ice. The monomer solution stock (1x PBS, 2 M NaCl, 2.5 % (w/v) acrylamide, 0.15 % (w/v) N,N'-methylenebisacrylamide, 8.6 % (w/v) sodium acrylate) was stored at -20 °C. When everything else was prepared APS and TEMED were added to the monomer solution stock (0.2 % each). The solution was vortexed briefly and then placed on the prepared stretchable foil as 50 µl drops. The coverslip with the sample was placed upside down on the drops. The samples were transferred for gelation to an incubator (Memmert, Schwabach , Germany), where it stayed for 60 min at 37 °C.

Digestion

The coverslip including the gelated sample was carefully detached from the foil and transferred to a six-well-plate. 2-3 ml Digestion buffer (50 mM Tris pH 8.0, 1 mM EDTA pH 8.0, 0.8 M Guanidine HCl, 0.5 % Triton X-100 (v/v) and freshly added Proteinase K (8 U/ml) were added to each well. Samples were left for digestion for 8 h.

Expansion

The gel was transferred into a petri dish with ddH2O for expansion. Water was changed at least 4 times. After 4 times 1.5 h in fresh water, gels were fully expanded.

2.2.4.2 ExM with expansion factor 10 (10xExM)

Anchoring

After immunolabeling of the samples, they were treated with Acryloyl-X, SE (0.1 mg/ml in PBS)

Gelation

Surface preparation: To obtain a flat surface for gelation, the cover of a petri plate was covered with stretchable semi-transparent foil. Monomer solution (2.67 % (w/w) DMAA, 0.64 % sodium acrylate) were bubbled for 40 min with N_2. 0.4 M KPS was added and solution bubbled with N_2 for 10 min. 0.004 %TEMED was added, then briefly vortexed and drops of each 50 µl added on the prepared stretchable foil. The coverslip with the sample was placed upside down on the drops. The samples were transferred to an N_2 flooded humid chamber, where they were left for 24 h at RT.

Digestion

The coverslip including the gelated sample was carefully detached from the foil and transferred to a six-well-plate. 2-3 ml Digestion buffer (50 mM Tris pH 8.0, 1 mM EDTA pH 8.0, 0.8 M Guanidine HCl, 0.5 % Triton X-100 (v/v) and freshly added Proteinase K (8 U/ml) were added to each well. Samples were left for digestion for 8 h.

Expansion

The gel was transferred into a big petri dish with ddH_2O for expansion. Water was changed 5 times after 1 h respectively. Last step should be over night, to allow the gel to fully expand.

2.2.4.3 Ultrastructure Expansion Microscopy (U-ExM)

Sample preparation

Sample preparation without immunolabeling.

Fixation and gelation

Coverslips with samples were incubated for 4-5 h at 37 °C in a solution of 0.7 % Formaldehyde and 1 % Acrylamide. Surface preparation: To obtain a flat surface for gelation, the cover of a six-well-plate was covered with stretchable semi-transparent foil. Gelation solution was prepared on ice. The monomer solution stock (1x PBS, 10 % (w/w) acrylamide, 0.1 % (w/w) N,N'-methylenebisacrylamide, 19 % (w/w) sodium acrylate) was stored at -20 °C. When everything else was prepared APS and TEMED were added to the monomer solution stock (0.5 % each). The solution was vortexed briefly and then placed on the prepared stretchable foil as 50 µl drops. The coverslip with the sample was placed upside down on the drops. For gelation the samples were transferred to an incubator (Memmert, Schwabach, Germany), where they were kept for 60 min at 37 °C.

Denaturation

The coverslip including the gelated sample was carefully detached from the foil and transferred to a six-well-plate. 2-3 ml Denaturation buffer (200 mM SDS, 200 mM NaCl, 50 mM Tris) were added and incubated 15 min at RT. When the gels have detached from the coverslip, the gels were transferred in a 1.5 ml tube with fresh denaturation buffer and incubated for 30 min at 95 °C.

Pre-expansion

Gels were transferred into petri plates and pre-expanded with ddH_2O (two times water change after 30min, then overnight at RT).

Labeling

Gels were washed two times for 15 min in PBS to get back gels from the original size. Next, gels were cutted in small pieces, which were immunostained in the following steps. Gel pieces were incubated in six-well-plates for 3 h with primary AB in 2 % BSA in PBS on a heating mat (TRIXIE Heimtierbedarf, Tarp, Germany) on a shaker running at 100 rpm (KM2, Edmund Bühler GmbH, Tübingen, Germany). Staining solution was discarded, and gels were washed three times for 10 min in 0.1 % Tween 20 in PBS on heating mat at 100 rpm. Afterwards, gels were incubated for 3 h with secondary AB in 2 % BSA in PBS on a heating mat at 100 rpm. Staining solution was discarded, and gels were washed three times for 10 min in 0.1 % Tween 20 in PBS on heating mat at 100 rpm.

Expansion

The six-well plates were filled with ddH_2O for the final expansion. Water was changed at least 4 times. After 4 times 1.5 h in fresh water, gels were fully expanded.

2.2.5 Imaging

2.2.5.1 Immobilization of the gel

To avoid movement of the gel sample on the coverslip during imaging, a gel piece was cutted out from the whole gel, put on a spatula and there carefully dried with wipes from the sides. Next, the gel was placed gently on a Poly-D-Lysine coated coverslip. After 10 min incubation time, water could be added to prevent the gel from drying out.

2.2.5.2 Setups

Imaging was performed mainly on two Setups. Unexpanded samples were observed on a Leica TCS SP8 confocal microscope, using a HC PL APO CS2 63x/1.20 water

objective (both from Leica Microsystems, Wetzlar, Germany). Expanded samples were observed on a Leica TCS SP5 confocal microscope with a resonant scanner, using a HCX PL APO CS 63x1.20 WATER UV objective (both from Leica Microsystems, Wetzlar, Germany).

Imaging using super-resolution microscopes was performed in the laboratory of Prof. Dr. Markus Sauer. Re-scan confocal microscope (RCM): Nikon TiE (Nikon, Japan), equipped with a 60x/1.27 water objective and Zyla 4.2P sCMOS camera from Andor. Structured-illumination microscope (SIM): Zeiss Elyra S.1 SIM equipped with a 63x oil objective (Carl Zeiss Microscopy, Jena, Germany).

2.2.5.3 Imaging

Images were acquired respecting the Nyquist criteria if not stated differently. For imaging stacks used for colocalization analysis, imaging was performed according to the settings described in Appendix part C.

2.2.6 Image Analysis

2.2.6.1 Deconvolution

Deconvolution was performed, using Huygens Professional 19.04 (Scientific Volume Imaging, Hilversum, The Netherlands). Settings: Background value was adjusted for images of unexpanded samples, using the preview window. For images, taken using the resonant scanner, no background value was set. Maximum iterations: 40; Signal to noise ratio: 20-30; Quality threshold: 0.05.

2.2.6.2 Colocalization Analysis

2.2.6.2.1 Channel alignment and chromatic aberration correction

Beads

For each channel and fluorophore combination, at least 30 images of 200 nm TetraSpeck™ beads were taken with the exact same settings as used for imaging the platelets. A median filter with radius 2 px was applied to every image in Fiji (ImageJ, National Institutes of Health, Bethesda, MD, USA).

ThunderSTORM

To evaluate the distortion in every part of the field of view, the images of each channel were merged, using the Fiji [50] plugin ThunderSTORM [51]. Settings used: Camera setup: Pixel size: according to images taken; No filter; Peak intensity threshold was adjusted to a value that only spots and no clots were visible. Other settings were left to default.

bUnwarpJ

To create a distortion matrix of each channel and align the channels, the Fiji plugin bUnwarpJ [52] was used.

Settings:	
Registration Mode:	Mono
Initial Deformation:	Coarse
Final Deformation:	Very Fine
Divergence Weight:	0.0
Curl Weight:	0.0
Landmark Weight	0.4
Image Weight	1.0
Stop Threshold:	0.01
Verbose:	Checked
Save Transformations:	Checked

At least 50 landmarks were set manually and connected to the corresponding spot in the other channel.

Macro for applying the distortion matrix to a big amount of data

The following macro was used to apply the distortion to every stack in a*.lif file, coming directly from the microscope:

```
setBatchMode(true);
path = File.openDialog("Select a File");
outpath=getDirectory("Choose a Directory");
run("Bio-Formats Macro Extensions");
Ext.setId(path);
Ext.getCurrentFile(file);
Ext.getSeriesCount(seriesCount);

for (s=1; s<=seriesCount; s++)
{
run("Bio-Formats Importer", "open=&path autoscale color_mode=Default
view=Hyperstack stack_order=XYCZT series_"+s);
Ext.getCurrentFile(file);
Ext.setSeries(s-1);
Ext.getSeriesName(seriesName);
Ext.getSeries(seriesName2);
Ext.getSeriesMetadataValue("Series 1 Name", value);
filename = getInfo("image.filename");
windowname = getTitle();
run("Split Channels");
selectWindow("C2-"+windowname);
Stack.getDimensions(width, height, channels, slices, frames);
run("Stack to Images");
selectWindow("C1-"+windowname);
run("Stack to Images");
for (i=1; i<=slices; i++)
```

```
{
call("bunwarpj.bUnwarpJ_.loadElasticTransform", "\\\\HC1008\\Users\\AG
Heinze\\Max\\DATA\\20190206_TS200nm\\A546_A488\\#Averaged shifted
histograms_A546_A488direct_transf.txt", "c:2/2 z:" + i + "/" + slices  + " - "+
seriesName, "c:1/2 z:" + i + "/" + slices  + " - " + seriesName);
selectWindow("c:1/2 z:" + i + "/" + slices  + " - " + seriesName);
setMinAndMax(0, 255);
run("8-bit");
}
run("Images to Stack", "name=StackC1 title=c:1/2 use");
run("Images to Stack", "name=StackC2 title=c:2/2 use");
run("Merge Channels...", "c1=StackC1 c2=StackC2");
run("Make Composite");
Stack.setDisplayMode("grayscale");
run("Arrange Channels...", "new=12");
outpath2 = outpath + filename + seriesName ;
run("OME-TIFF...", "save=["+outpath+filename+seriesName+".ome.tif] export
compression=Uncompressed");
}
```

2.2.6.2.2 Colocalization Analysis using Imaris

After deconvolving the images according to chapter 2.2.6.1, Imaris 9.2.1 (Bitplane AG, Zurich, Switzerland) was used to calculate the colocalization between two channels. But before the colocalization analysis, every single platelet was cropped and saved separately. For the colocalization analysis the threshold was set to 2 and the Pearson coefficient of every platelet was noted manually.

2.2.6.3 Receptor counting

To estimate the number of receptors per platelet, a workflow was developed to count the number of events in one platelet. All following steps were performed using Imaris 9.2.1 (Bitplane AG, Zurich, Switzerland). The surface module was used to modulate small surfaces in every spot.

Settings:	
Smooth	Checked
Background Subtraction (Local contrast)	Checked; 0.400 µm
Threshold (Background subtraction)	10.6
Split touching Objects	Checked; 0.200 µm
Seed Point Filters	Intensity Mean above 20.0
Classify Surfaces Filters	Numbers of Voxels above 40.0

2.2.6.4 Platelet surface area and volume

To calculate the receptor density in platelets, the platelets surface area and volume were estimated, using the Cell Module of Imaris 9.2.1.

Settings:	
Detection Type	Detect Cell only Detect Cell boundary from Cytoplasm
Smooth	Checked; 0.5 µm
Cell Threshold	Adjusted so that the whole platelet was marked

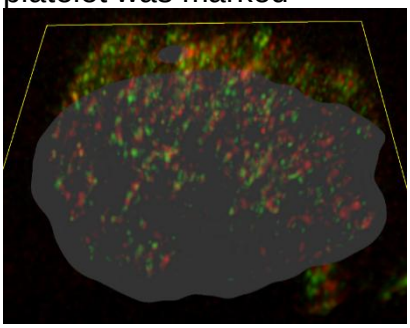

Figure 13: Cell threshold adjustion. Imaris 9.2.1

For some platelets, this workflow failed. Then following settings were used in the Cell Module instead:

Settings:	
Detection Type	Detect Cell only Detect Cell boundary from Cell Membrane
Cell smallest diameter	5.0 µm
Membrane Detail	0.5 µm
Filter type:	Smooth
Cell Membrane Threshold & Classify Cells Filters	Adjusted so that the whole platelet was marked

Since some platelets were cut off at the bottom during imaging, the ‘missing’ area was calculated and subtracted from the surface area. All voxels in the previously modulated cell were masked to intensity 100 in a new channel. With the surface module, a surface 1 voxel thick was created where the platelet was cut off. Half of the created surface area was subtracted from the platelets surface area.

2.2.7 Statistical analysis

Statistical analysis was performed using Origin 2019 (OriginLab Corporation, Northhampton, United States). Normality was tested using Shapiro-Wilk test. According to the results, One-way ANOVA followed by Student’s t-test with Bonferroni correction, or Kruskal-Wallis test followed by Mann-Whitney-U test with Bonferroni correction were performed. Significance level was set to 0.05.

2.2.8 Fluorescence-Activated Cell Sorting (FACS)

Washed platelets were adjusted to a concentration of 500,000/µl. For live staining: 150 µl platelet suspension were mixed with 60 µl antibody and 90 µl Tyordes -Ca^{2+} and incubated at 37 °C. After 2, 10- or 30-min staining duration, 50 µl of the suspension was diluted in 200 µl Glyoxal-buffer and centrifuged at 2,800 rpm for 5 min and afterwards resuspended in 500 µl PBS. For post-fixation staining: platelet suspension (500,000/ µl) was diluted 1:1 in Tyrodes -Ca^{2+}. 150 µl of the suspension were mixed with 600 µl Glyoxal-buffer and incubated for 10 min at 37 °C. The suspension was centrifuged at 2,800 rpm for 5 min and resuspended in 120 µl Tyrodes -Ca^{2+} and 30 µl antibody. After 2, 10 or 30 min, 50 µl of the suspension was diluted in 400 µl PBS, centrifuged at 2,800 rpm for 5 min and resuspended in 500 µl PBS. The MFI was measured using a FACSCelesta (BD Biosciences, San Jose, USA).

3 Results

With the objective to improve the imaging of membrane receptor distributions by using ExM, this thesis provides first results towards this goal. In this chapter, in the beginning I am going to outline which changes in the protocol lead to improved image quality for 4xExM and show results regarding 'Live staining', cytoskeleton staining and imaging of activated platelets. Furthermore, I show the results of the antibody characterization for ExM regarding different antibodies. After optimizing the 4xExM protocol, I tried to use the 10xExM and U-ExM protocol for imaging platelet receptors, as well as I used super-resolution setups for imaging expanded samples. Finally, an event number analysis and colocalization analysis show first steps towards resolving receptor distributions.

3.1 ExM with expansion factor 4 (4xExM)

3.1.1 Introducing Glyoxal and Acryloyl-X in the protocol for brighter images

In a first step, the expansion protocol needed to be adjusted and optimized for platelets, since this new technique has not been applied on platelets before. Every cell or tissue type has different properties and requirements when it comes to ExM and this entailed changes in the key reagents and procedures of the original ExM protocol [8]. Richter and co-authors [53] introduced Glyoxal as a faster and better fixative, mainly regarding preservation of fluorescent intensity, compared to PFA [8]. In an experiment, the fixatives PFA (4 %), PLP, Glyoxal and CS-Buffer (contains 2% Glutaraldehyde) were compared on unexpanded platelets regarding fluorescent intensity. As shown representatively in **Figure 14** in a comparison between Glyoxal and PFA, Glyoxal outperformed the other fixatives (see the comparison between PFA, Glyoxal, PLP and CS-Buffer in Appendix Part A).

After fixation, the linking of the sample and fluorophores into the gel is achieved by equipping these structures with a free acrylamide end, which during the gelation step will be integrated into the growing gel matrix. Tillberg and co-authors [37] used Acryloyl-X (AcX) instead of the originally used Glutaraldehyde for this linking step. Applied on platelet samples, AcX showed three advantages: brighter signal, less unspecific signal 'inside' the platelet and a better-preserved ring structure of the imaged platelet (**Figure 15**).

The 4xExM protocols were adapted accordingly to these results, consequently using Glyoxal for fixation and Acryloyl-X for linking.

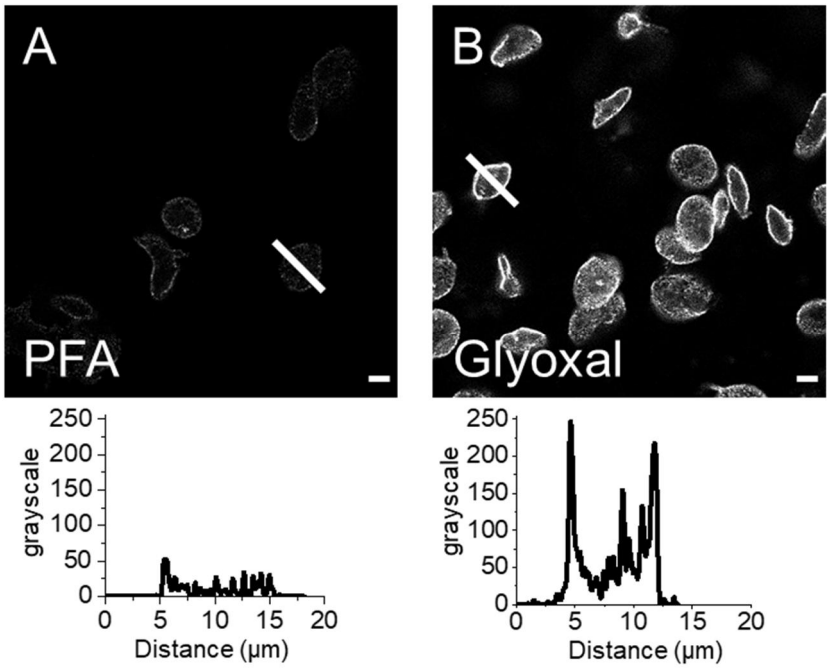

Figure 14: Glyoxal fixation increases fluorescent intensity. Confocal images of 4x expanded resting platelets which were fixed with PFA **(A)** and Glyoxal **(B)**, stained with anti-GPIX (56F8IgG-A594) and afterwards linked into the gel using Acryloyl-X. The intensity plots along the marked lines show higher fluorescence intensity for Glyoxal than for PFA. Scale bar: 5 µm

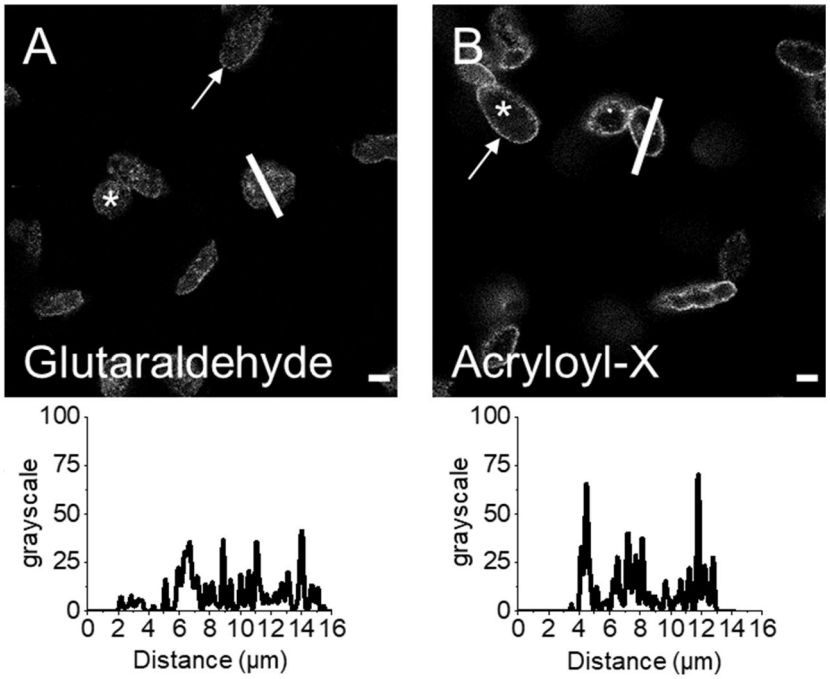

Figure 15: Acryloyl-X linking increases fluorescent intensity and reduces unspecific signal. Confocal images of 4x expanded resting platelets which were stained live with anti-GPIX (56F8IgG-A594), fixed with Glyoxal and linked with Glutaraldehyde **(A)** and AcX **(B)** to the gel. The intensity plots show a higher signal level for AcX in comparison to Glutaraldehyde. Furthermore, AcX shows less unspecific signal (star) with better preserved ring structure (arrow). Scale bar: 5 µm

3.1.2 Showing the feasibility of ‘Live staining’ in ExM

The binding of (fluorophore-coupled) antibodies can initiate processes like clustering or internalization in the platelet and hereby for example lead to platelet activation. For the GPIIb/IIIa receptor, an internalization of anti-GPIIb/IIIa antibodies upon binding to the corresponding binding site has been described [54]. To image these processes, platelets can be stained before fixing (‘live staining’) and thereby be fixed in the modified state. Using ‘live staining’, I was able to show that ExM is able to image receptor internalization in platelets (**Figure 16**).

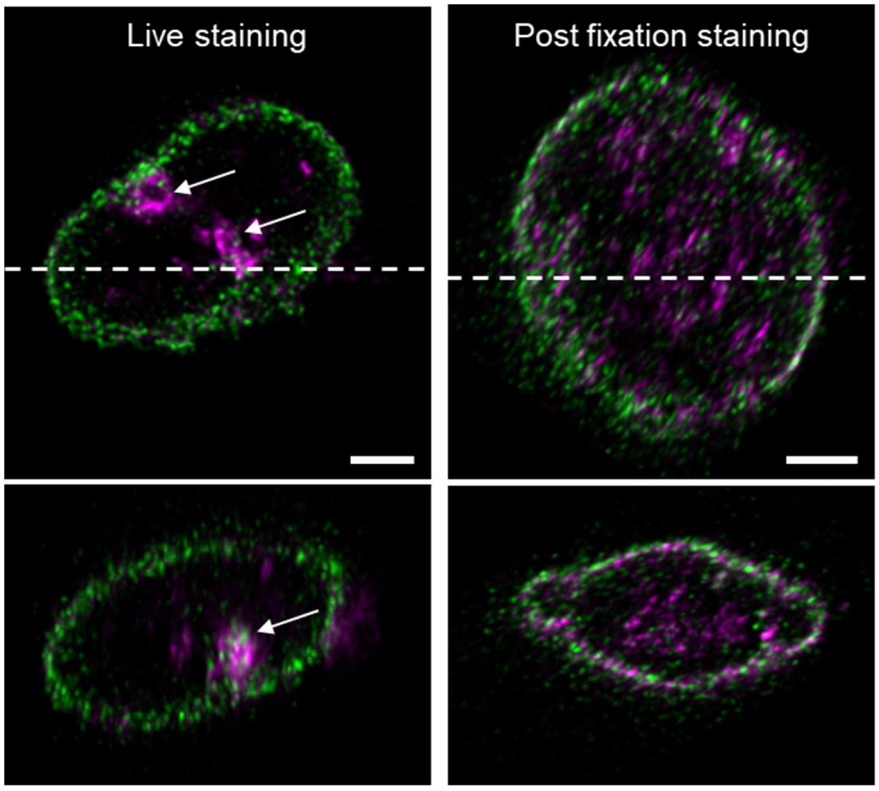

Figure 16: Receptor internalization upon anti-GPIIb/IIIa antibody binding: xy- (above) and xz-image (below) sections (indicated by white dotted lines) of 3D confocal image stacks of 4x expanded live (left) and post fixation stained (right) resting platelet. When the anti-GPIIb/IIIa antibody (magenta, 5D7IgG-A488) attaches to the receptor, receptor internalization is induced, visible as magenta clusters inside the live stained platelet (arrows). To visualize the platelets membrane, GPIX was also stained (green, 56F8IgG-A594). Scale bar: 3 µm

3.1.3 Cytoskeleton/intracellular staining

As mentioned before, ExM could make colocalization studies between the cytoskeleton and membrane receptors feasible and hereby lead to interesting findings. As a groundwork for this project, it was necessary to evaluate the practicability of simultaneous membrane and cytoskeleton staining. This is challenging because the labels directed to the cytoskeleton needs to be transported through the membrane without destroying it. Permeabilization, using Cytosceleton Buffer (CS-Buffer) which contains Triton-X100 resulted in images where the membrane staining did not work well anymore. It appeared that the antibodies were not able to bind their epitopes and consequently in the images the membrane looked scattered and has barely existing fluorescent intensity (**Figure 17**).

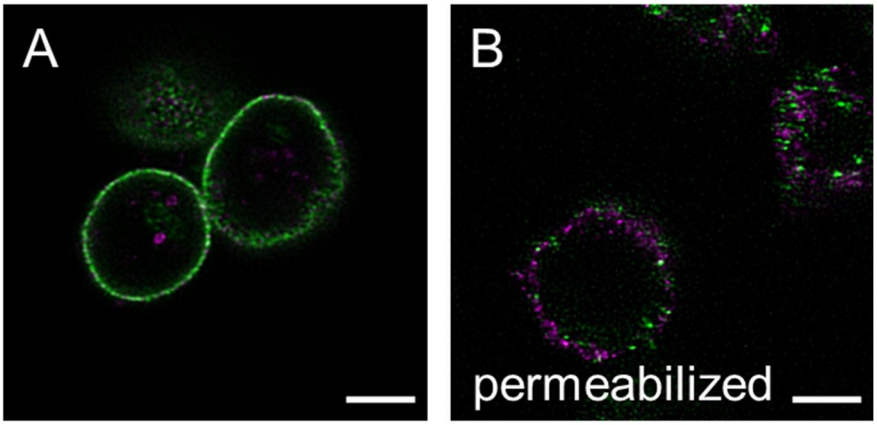

Figure 17: Using Triton-X100 for permeabilization makes imaging of membrane receptors impossible. Confocal images of 4x expanded resting platelets which were fixed with Glyoxal, stained with anti-GPIX (green, 56F8IgG-A594) and anti-GPIIb/IIIa (magenta, 5D7IgG-A488) and linked with AcX. When permeabilizing the platelets membrane with 0.1 % Triton-X100 **(B)**, membrane structure and most of the fluorescent intensity is lost. Compared to the control **(A)**,the laser intensity was increased 10 fold (from 5 to 50 %) and the image brightness in post-processing also was increased 1.5 fold. Scale bars: 5 µm

According to this results, Triton-X100 does not seem to work for a membrane preserving staining. The use of Glyoxal-buffer showed also permeabilizing features, which could be traced back to the 19.9 % Ethanol ratio contained. In **Figure 18** the permeabilizing effect of Glyoxal-Buffer is shown in a simultaneous cytoskeleton (actin) and membrane-stained sample. These images suggest that Glyoxal permeabilizes the membrane enough to allow intracellular labeling without the destruction of the membrane.

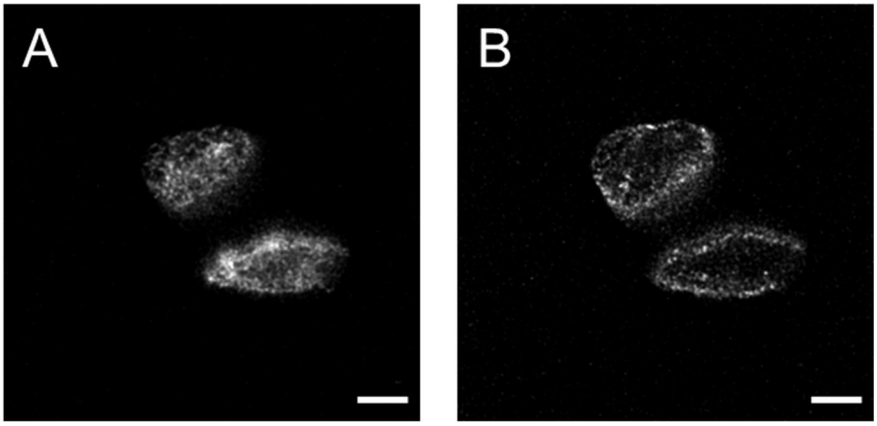

Figure 18: Permeabilizing effects of Glyoxal-Buffer. Separated channels of a confocal image of 4x expanded resting platelets which were fixed with Glyoxal, stained with Phalloidin (**A**, Actin ExM A561) and anti-GPIX (**B**, 56F8IgG-A488) and linked with AcX. The images suggest, that Glyoxal has slight permeabilizing properties without harming the membrane, since F-actin and the membrane receptor GPIX can be imaged in the same platelets without the use of other permeabilizing reagents. Scale bars: 5 µm

3.1.4 Towards imaging activated platelets using ExM

Next, we aimed for imaging activated platelets. Thus, we stimulated platelets with thrombin, an agonist of the murine PAR-receptor against thrombin, before letting them settle on fibrinogen coated coverslips. Fibrinogen enhances the activation of the platelets as it covalently links to integrins in the membrane and thus assures full activation before the fixation step. This experiment has only been performed once, but it appeared that the link between the activated platelet and the fibrinogen coated coverslip is very strong so that the platelets are ripped out of the gel when detaching the gel from the coverslip. To allow imaging of activated platelets, I showed in unexpanded samples that activated platelets would also settle on Glycine coated coverslips as they were used for resting platelets (**Figure 19**). As shown in 3.1.5.3, Glycine coated coverslips also allow the imaging of activated, expanded platelets, therefore this strategy can be pursued for further experiments.

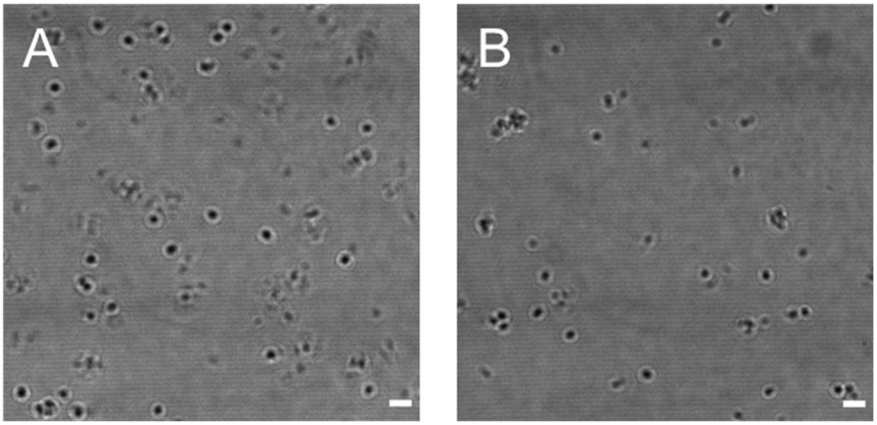

Figure 19: Activated platelets settle on Fibrinogen and Glycin coated coverslips. Transmitted light microscope image of not expanded activated platelets. Activated platelets settled on both Fibrinogen coated coverslips (A) and Glycin coated coverslips (B). While activated platelets form strong connections with the Fibrinogen, preventing the platelets to detach from the coverslips when detaching the gel, the use of Glycin coated coverslips makes imaging of activated platelets feasible. Scale bar: 5 µm

3.1.5 Antibody characterization for ExM

The impact of ExM for platelet research strongly relates to the compatibility of a variety of different platelet antibodies with the ExM protocol. I pinpointed how long the sample should be incubated with various antibodies to reach full antibody saturation with lowest possible unspecific binding and noise and established a library of platelet antibodies suitable for ExM. Furthermore, the use of Fab-Fragments, which – as explained before - promise a lower linkage error, and reagents for cytoskeleton staining in ExM were tested. All antibodies covered in this chapter were labeled by the AG Nieswandt (RVZ Würzburg, Germany) and cover different clones of the receptors GPIbα (57E12, 15E2, 92H12, 7A9) , GPIbβ (3G6), GPIIb/IIIa (5D7, 14A3, 4H5, 45A9), GPIIIa (57B10) and GPIX (56F8). For more information about the antibodies used, see 2.1.3.

3.1.5.1 Evaluating different staining durations for the ExM protocol

The time a specimen is incubated with a fluorescent antibody always entails a tradeoff between labeling all available epitopes and minimizing unspecific binding. Here, we evaluated the optimal staining duration for anti-membrane receptor antibodies in live cell and post-fixation labeling. In live staining, labeling takes place in a platelet suspension and the antibodies can access their epitopes very fast and without obstacles. Therefore, the platelets are fully saturated with antibodies in a very short time. When staining fixed platelets, fractions of the fixative are impeding an easy access of the antibody to the epitope, sometimes making an epitope not accessible. Hence, the staining duration to get full receptor saturation in post-fixation labeling in

general is longer. To minimize unspecific artefacts and noise, the staining duration should be as short as possible. To evaluate the epitope saturation over time and to improve our staining protocol, the fluorescence intensity of the fluorophore attached to the antibody was measured after 2, 10 and 30 min of staining. The staining experiment was performed for live and post-fixation stained platelets. The mean fluorescent intensity (MFI) was analyzed using fluorescence-activated cell sorting (FACS). This experiment was performed by Vanessa Klaus (AG Stegner, RVZ Würzburg).

The results presented in **Figure 20**, show the relative intensity of the time points 2 and 10 min compared to 30 min. For post-fixation staining, it was visible that none of the antibodies was fully saturated after 2 min and the intensity was rising until 30 min. For live stained platelets, the staining duration did not play a role as big as in post-fixation staining. Most of the receptors were saturated very fast, except for 4H5.

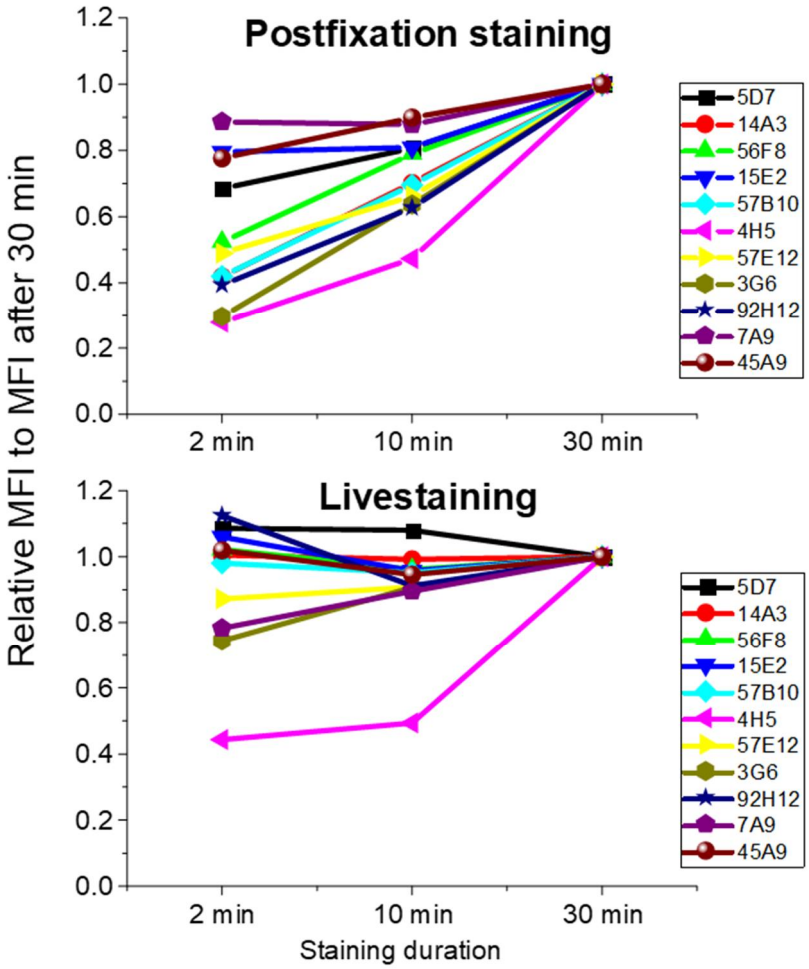

Figure 20: Relative Mean Fluorescent Intensities (MFIs) after different staining durations. Live- and postfixation stained platelets were stained with different staining durations and each MFI was compared to the MFI after MFI after 30 min (= 1). In post-fixation staining, the relative MFI varies a lot between different antibodies, whereas in livestaining, the platelets are mostly saturated very fast.

3.1.5.2 Comparing the compatibility of different antibodies and F_{ab}-fragments against membrane receptors with ExM

During the performed experiments, the antibodies used showed a wide variability in their affinity and fluorescent intensity. Therefore, it became necessary to create a library of suitable antibodies against platelet receptors, which are compatible with the ExM protocol. Especially F_{ab}-fragments needed to be checked for their compatibility, since they come with a lower density of labeling (number of fluorophores per F_{ab}-fragment), potentially resulting in more dim images, but the advantage of a smaller linkage error compared to IgG antibodies, what could play an important role when imaging at higher resolutions, especially in 10xExM. All platelet antibodies and F_{ab}-fragments of interest were imaged in unexpanded platelets with the same settings (Images of every antibody and F_{ab}-fragment see Appendix Part B). Their applicability for ExM was rated subjectively respectively the obtained brightness of the image. All Antibodies and F_{ab}-fragments were categorized in Table 1 into four groups (++ good, + okay, - bad, -- very bad) according to **Figure 21**. Furthermore, for expanded platelets I complemented Table 1 with the subjective performance each antibody showed in the experiments during my experimental period.

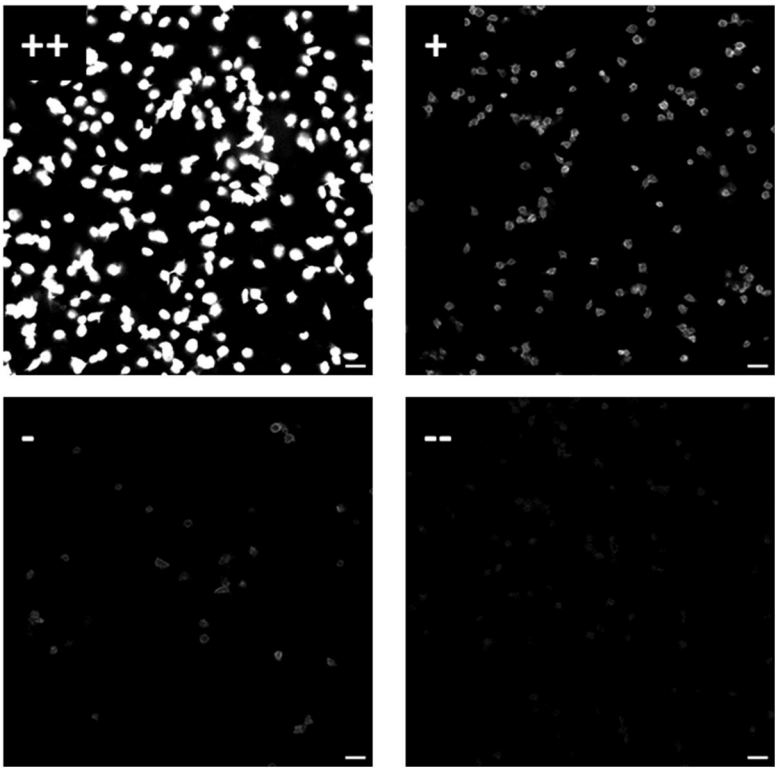

Figure 21: Classification of the applicability of antibodies and F_{ab}-fragments for ExM. Based on confocal images of unexpanded resting platelets, the antibodies were rated regarding the image brightness. Hereby they were sorted subjectively for their applicability with ExM into four groups: **++** good; **+** okay; **-** bad; **--** very bad. Scale bar: 5 µm

Table 1: List of available antibodies and F_{ab}-Fragments

Antibody	**Unexpanded**		**Expanded**	
	Live staining	Postfix staining	4xExM	10xExM
GPIbα				
57E12 Fab A488	**-**	**(+)**	**-**	n.d.
15E2 Fab A488	**-**	**-**	**- -**	n.d.
15E2 IgG A488	**-**	**-**	**-**	n.d.
15E2 Fab Atto647N	**+**	**+**	**- -**	n.d.
92H12 IgG A488	**- -**	**-**	**- -**	n.d.
92H12 IgG A546	**- -**	**-**	n.d.	n.d.
GPIbβ				
3G6 IgG A488	**+ +**	**+ +**	n.d.	n.d.
3G6 IgG A594	**+ +**	**+ +**	n.d.	n.d.
GPIIb/IIIa				
5D7 IgG Atto647N	**+ +**	**+ +**	**-**	n.d.
5D7 IgG A488	**+ +**	**+**	**+**	**+**
5D7 Fab A532	n.d.	**+**	**+**	n.d.
14A3 IgG A546	n.d.	**+ +**	**+**	n.d.
14A3 IgG A488	n.d.	**+**	**+**	n.d.
GPIX				
56F8 IgG Atto647N	**+ +**	**+ +**	n.d.	**- -** (1 try)
56F8 IgG A594	**+ +**	**+ +**	**+**	**+**
56F8 IgG A488	**+**	**+**	**+**	n.d.

Summarizing these results, it can be said that we have a big variety of suitable antibodies against different receptors. Currently, the GPIbα receptor is the only receptor lacking an antibody bright enough to obtain evaluable images after expansion. I was also able to show that F_{ab}-Fragments in general work (5D7F_{ab}-A532), but for the GPIbα receptor, where we are prospectively interested in doing colocalization analysis with the actin filament, none did work.

3.1.5.3 Tubulin and Actin Skeleton staining

As mentioned before, a future aim is to do colocalization studies between Cytoskeleton and membrane receptor. Therefore, suitable labels were needed, which survive the ExM protocol.

Monoclonal anti-β-Tubulin delivered nice pictures of the microtubule system and even worked using the 10xExM protocol as shown in **Figure 22.A**, where clearly the tubulin ring structure of the platelet is visible. For staining of actin filaments, monoclonal anti-beta-actin antibodies did not work with platelets in ExM, but good results could be achieved using a linkable phalloidin derivate (Actin ExM, Chrometra, Belgium). **Figure 22.B** shows a cluster of densely packed activated platelets with outstretched actin filopodia.

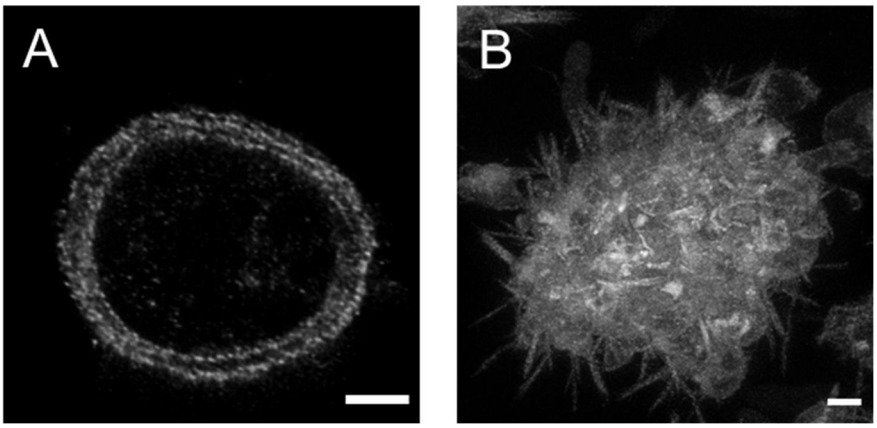

Figure 22: Intracellular staining of Tubulin and Actin. (A) Confocal image of a 10x expanded resting platelet stained with anti-β-tubulin. **(B)** Confocal image of 4x expanded cluster of activated platelets stained with 'Actin ExM'. Scale bars: 5 µm

3.1.5.4 Evaluating the labeling specificity

To see how much unspecific signal is produced by the fluorescent antibodies, an experiment with knockout (KO) platelets was performed. KO platelets are lacking a certain receptor and therefore all bindings of the corresponding antibody are unspecific. In **Figure 23** it is possible to see that in GPIbα-KO platelets, after anti-GPIbα staining - in contrast to wildtype (WT) platelets - nearly no unspecific signal was visible.

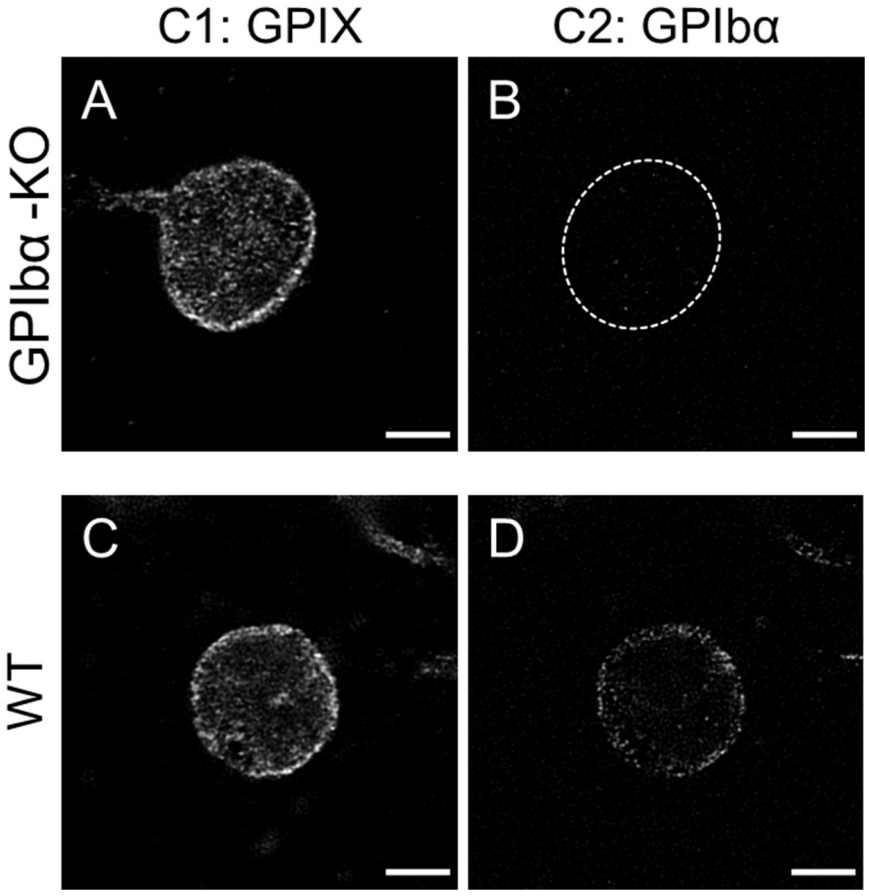

Figure 23: Knockout platelets show low unspecific fluorescent signal. Confocal image of 4x expanded resting platelets stained with anti-GPIX (56F8IgG-A594) and anti-GPIbα (15E2IgG-A488). Nearly no unspecific signal was visible in the GPIbα-channel of the GPIbα-KO platelets. The dotted line displays the position of the platelet, determined from the GPIX-channel. The GPIbα signal of wildtype platelets is dim due to poor antibody properties, but clearly visible. Scale bars: 5 µm

3.2 Testing new protocols: ExM with expansion factor 10 (10xExM) and Ultrastructure ExM (U-ExM)

Since expansion microscopy is a relatively new method, a lot of effort needs to be put on improved protocols and experimental tweaks to overcome bottlenecks in sample preparation. The results presented above were all based on the original ExM approach with expansion factor 4 (4xExM). During or shortly before my experimental work on this thesis, two new different protocols of ExM were published, bringing new possibilities in comparison to the original Protein retention microscopy (proExM or 4xExM) [37]:

- ExM with expansion factor 10 (10xExM) [41]
- Ultrastructure expansion microscopy (U-ExM) [39]

Table 2 shows the different protocols and highlights the main differences, which will be explained in detail later.

Table 2: Comparison of Expansion protocols

	4xExM	**10xExM**	**U-ExM**
Labeling	Pre-gelation		Post-gelation
Linking	Acryloyl-X		Formaldehyde & Acrylamide excess
Digestion/ Denaturation	Proteinase K @ RT	Proteinase K @ 50 °C	SDS @ 95 °C
Expansion factor	4x	10x	4x

3.2.1 ExM with expansion factor 10 (10xExM)

The 10xExM protocol provides a dramatic resolution gain. The gel ingredients are different from previous protocols [41] and allow the gel to expand by the factor of 10. However, the 10xExM protocol is accompanied by a bigger loss of intensity compared to 4xExM, due to two reasons: 1. The digestion with Proteinase K needs to be performed at 50 °C instead of at room temperature. This is necessary to allow a homogeneous expansion but destroys more fluorophores. 2. All fluorophores are pulled further apart, since the volume of the sample increases by the factor 1000, while in 4xExM only by the factor 64. The results, exemplary shown in **Figure 24** suggested,

that nevertheless, 10xExM delivered sufficient fluorescent intensity, to be used with blood platelets. Of course, laser intensities and imaging settings needed to be adjusted according to the dimmer samples. But since simply by looking at the image or by comparing signal intensities it is not possible to tell if 10xExM is superior to 4xExM. A way to quantify this comparison would be for example to perform colocalization analysis experiments as described in 3.4.2 with 4xExM and 10xExM.

The handling of 10xExM gels was very difficult and needs more training in comparison with the straight-forward handling of the 4xExM gels. Moreover, the reproducibility of consistent gel properties between the different experiments was much lower in 10xExM compared to 4xExM, although the protocol was carried out exactly as described in the original paper. I suspect that remaining oxygen in the gel is accountable for this, preventing efficient and homogeneous gelation. Maybe a modified setup in the lab with better possibilities to exclude oxygen from the experiment could help.

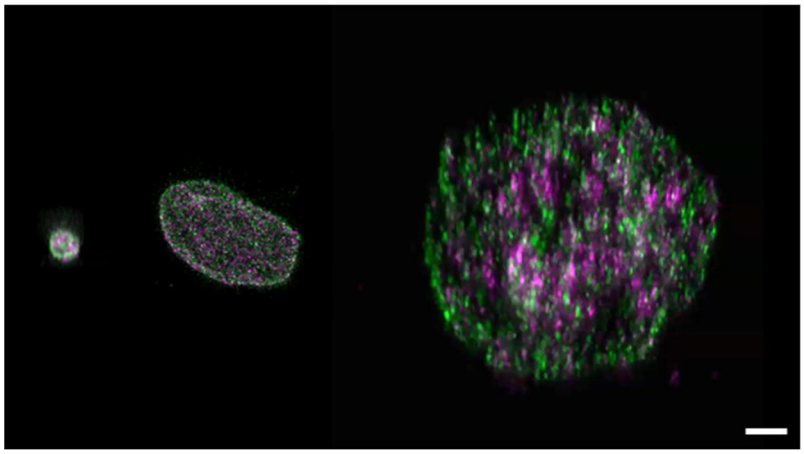

Figure 24: Size comparison between unexpanded, 4xExM and 10xExM platelets. Confocal image of unexpanded (left), 4x expanded (middle) and 10x expanded (right) resting platelets stained with anti-GPIX (green, 56F8IgG-A594) and anti-GPIIb/IIIa (magenta, 5D7IgG-A488). Scale bar: 5 µm

3.2.2 Ultrastructure expansion microscopy (U-ExM)

The biggest advantage of the U-ExM protocol is the post-denaturation and gelation labelling of the sample. The sample is denaturated by Sodium Dodecyl Sulfate (SDS) at 95 °C. SDS only denaturates the proteins and does not digest them like Proteinase K, so that some epitopes should still be preserved afterwards. Since the sample is stained after the denaturation process, the antibodies are not exposed to any detergents with the result that a brighter sample is received. With Chinese hamster ovary cells (CHO-cells) this protocol worked in our hands and delivered bright images although the stained tubulin wasn't visible in the expected regular tubular structure (**Figure 25**). However, for platelets it was not possible to establish this protocol during my experimental work. U-ExM with platelets resulted in samples with no detectable signal at all, most probably due to antibodies which are not able to bind after the denaturation with SDS.

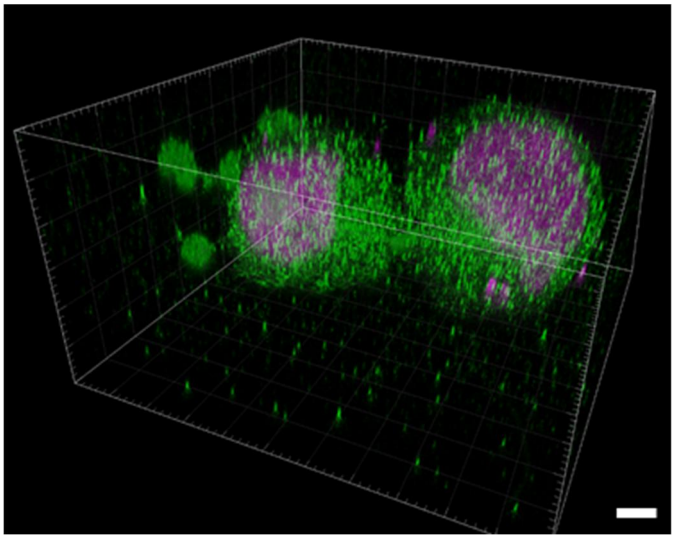

Figure 25: Ultra-ExM protocol with CHO cells. For CHO cells the Ultra-ExM protocol worked well and delivered bright pictures of Tubulin (green) and DNA (Hoechst, magenta). Scale bar: 10 µm

3.3 ExM in combination with other super-resolution imaging approaches

For even higher resolutions, ExM samples can be observed by using super-resolution microscopes. Requirements for suitable microscopy are the support of 3D imaging and multi-color imaging. The use of Re-scanning confocal microscopy (RCM) and Structured Illumination Microscopy (SIM) was tested on expanded platelets.

In **Figure 26**, platelets imaged with RCM are compared to conventional confocal imaged platelets. The RCM images show good contrast but low signal-to-noise ratio (4.5 compared to 9.8 in the confocal image).

In **Figure 27**, a SIM image is compared to an image taken with a conventional confocal microscope. Since SIM images are created with high computational effort, the compared confocal image is deconvolved. The weak fluorescent intensity of the sample resulted in SIM images with low signal to noise ratio and lots of artifacts with stripe pattern.

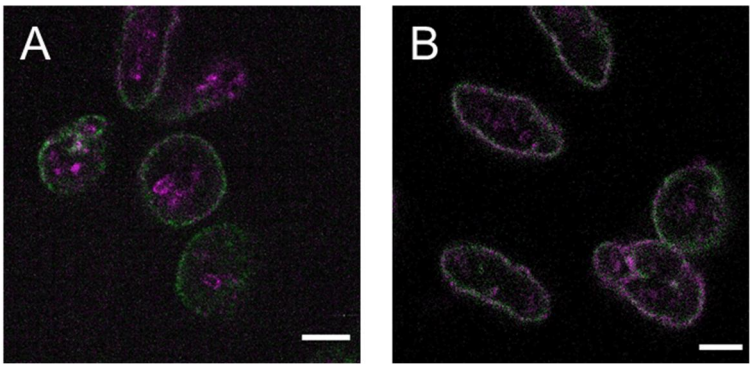

Figure 26: ExM in combination with Re-scanning confocal microscopy. The image of the Re-scanning confocal microscope (A) was compared to a confocal image (B). The Re-scanning microscope image shows good contrasts and has a Signal-to-Noise ratio of 4.5 compared to 9.8 in the confocal image, what shows the superiority of the confocal microscope. Scale bars: 5 µm

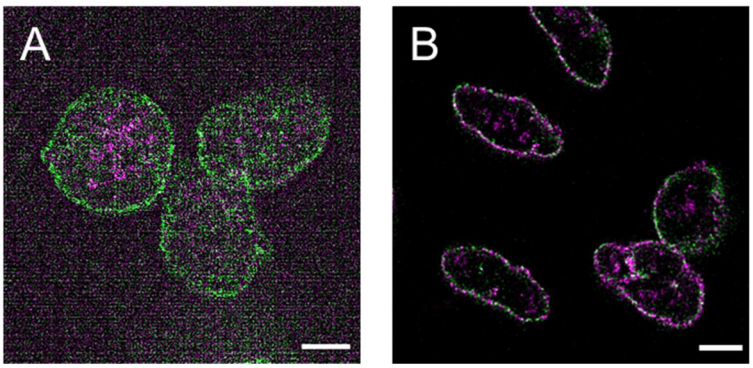

Figure 27: ExM in combination with 'Structured Illumination Microscopy'. The SIM image (A) exhibits artefacts due to low image contrast. The deconvolved confocal image (B) shows the current superiority of confocal microscopy. Scale bars: 5 µm

3.4 Towards resolving receptor distributions on blood platelets

Is ExM enabling us to image the distribution of membrane receptors and receptor interactions and thereby giving us more insight into the mechanisms of platelet function? The resolution advantage of ExM towards conventional fluorescent microscopy is already easily visible with the unaided eye but this advantage needed to be quantified and qualified to come to a valid conclusion.

Hence, platelets of three different staining combinations as shown in **Figure 28** were prepared and stacks of single platelets were imaged (Imaging parameters see Appendix part C) and analyzed (2.2.6). The dual-color experiments covered three different staining scenarios, which represented one case for which the highest possible colocalization was expected and two for which no colocalization was expected. Highest possible colocalization was expected in case (I) simply because both fluorophores are bound to the same receptor on different epitopes. No colocalization was expected for case (II) and (III). In case (II) one epitope was simultaneously stained with 2 different fluorophores so that 50% of the epitopes were covered with one color, 50% with the other one. In case (III) two supposedly not interacting receptors are distinctly labeled. The choice of cases should give important measures about the dynamic range of colocalization analysis using ExM approach on platelets.

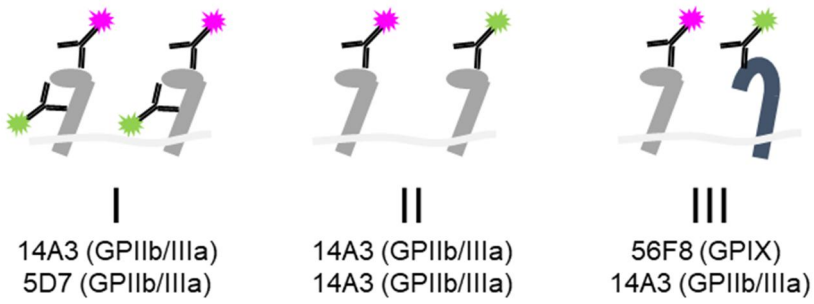

Figure 28: Labeling scenarios to resolve receptor distributions. Staining case I: two different Epitopes (14A3IgG-A546, 5D7IgG-A488) on the GPIIb/IIIa receptor labeled with one color each. Case II: One Epitope labeled with one of the fluorophores (14A3IgG-A546, 14A3IgG-A488) on the GPIIb/IIIa receptor. Case III: Complementary labeling of the GPIIb/IIIa (14A3IgG-A488) and GPIX (56F8IgG-A59) receptor.

3.4.1 Event number analysis

Based on the different staining cases explained in 3.4, the following can be assumed: If an imaginary platelet is stained once with Staining I and (the exact same platelet) once with Staining II, the total amount of events imaged ('dots') in both colors summarized should be double in case I compared to case II. The reason is that in case I each receptor is occupied by two antibodies, whereas in case II it is only one antibody (**Figure 29**).

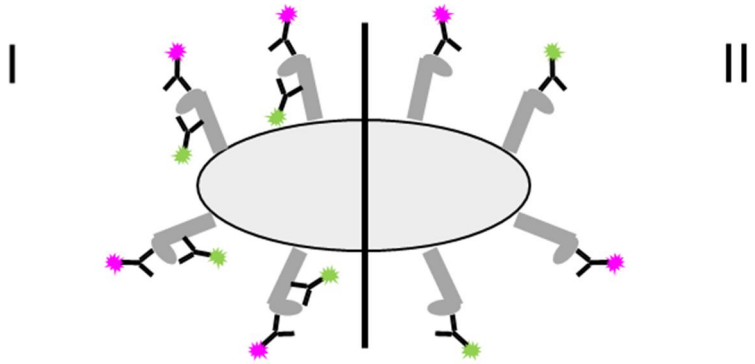

Figure 29: Different stainings applied on the same platelet. In Staining case I, each GPIIb/IIIa is occupied by two antibodies, whereas in case II every receptor is only occupied by one antibody, but half of them from one color, the other half from another. Theoretically, the total amount of binding antibodies in case I is doble the amount in case II. These amounts can be determined, when analysing the event count.

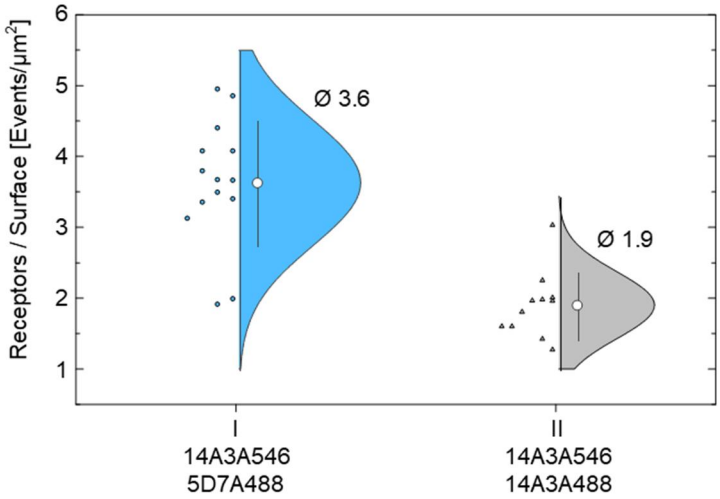

Figure 30: Comparison of the receptor density of GPIIb/IIIa between staining case I and II. To obtain the receptor density, visible events ('dots') of both channels (two colours) were analysed, counted and divided through the platelets surface area. The result with I = 1.9xII is close to the prediction I = 2xII.

Because the number of events varies with the size of a platelet, the event density (events per platelets surface area) was calculated to make the results comparable among different platelets. Theoretically the total event density of case I should be

double the receptor density of case II (I = 2x II). **Figure 30** shows, that with I= 1.9x II, the results are close to this hypothesis.

The data also delivered information about the loss of the different fluorophores used. Comparing the number of events in each channel from one platelet, it becomes possible to make statements about the survival of fluorophores during the ExM protocol. In **Figure 31**, it is shown how much percent more or less events of A488 fluorophore were counted, compared to A546 fluorophores. For case II, where the same antibody with different fluorophores was used, it is clearly visible that the Alexa488 fluorophore is digested more than Alexa546 (Image B in **Figure 31**). In case I, both fluorophores (Alexa488 & Alexa546) are detected with the same counts, which could mean that the 5D7 antibody (which was coupled to the Alexa488 fluorophore) has a higher affinity than 14A3 (Image A in **Figure 31**).

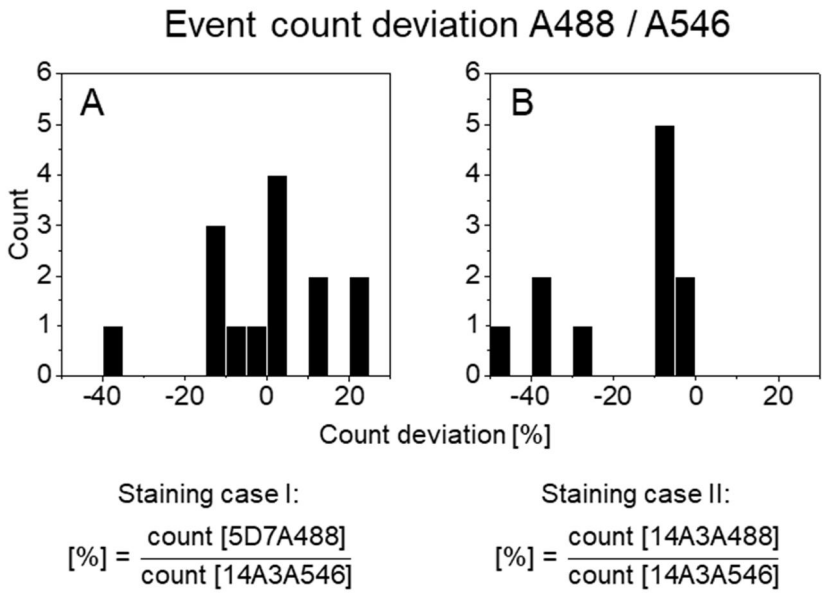

Figure 31: Post-expansion difference in the event count of Alexa488 and Alexa546 attached to the same receptor. GPIIb/IIIa receptors were stained at 2 epitopes with different colors. Event counts were analysed for both channels separately and displayed as count number of Alexa488 in relation to Alexa546. In **(B)** with staining case II, it is visible that Alexa488 is digested more since the same Antibody is used. In **(A)** it is visible that Alexa488 and 546 has the same count numbers. Assumed, Alexa488 is digested more, 5D7A488 could have a stronger affinity to the associated epitope.

3.4.2 Colocalization analysis

Colocalization analysis is a tool that derives information about the relationship and interaction between two molecules, compartments or (cellular) structures by the spatial overlap of two fluorescent labels of distinct color channels. To evaluate, if the resolution gain using ExM results in better colocalization analysis results, Pearson coefficients of the three staining cases as shown in chapter 3.4 were determined for 4x expanded and not expanded samples. The labelling strategy was chosen to cover both full colocalization (Case I) and no colocalization (Case II and III). Case I is the positive control and should show high colocalization with a high Pearson coefficient by labeling two different epitopes on the same receptor. Case II and IIII are negative controls and should show no colocalization with a low Pearson coefficient by labeling one epitope simultaneously with two different fluorophores (II) and by labeling different receptors (III).

As shown in **Figure 32** the use of 4xExM improves the dynamic range of the measured results significantly. With a theoretically expected dynamic range of the Pearson coefficient from 0 to 1, the results implicate that 4xExM offers a dynamic range from 0.11 to 0.73 (blue) to quantify the colocalization of membrane receptors while normal confocal microscopy only offers 0.71 to 0.79 (grey). With n=50 for each case, the results among unexpanded and expanded platelets were significantly different among each other. For the statistical analysis, see Appendix part D. The measured values in case I of 0.79 for unexpanded platelets and 0.73 for 4x expanded platelets fit to the expected Pearson coefficient of 1 when considering the loss of fluorophores and other influences like small inaccuracies of the microscope. To check, if 0.73 respectively 0.79 is the highest achievable Pearson coefficient the antibodies could be labelled with a fluorophore coupled secondary antibody. Thereby, the fluorophores of the primary and secondary antibody should be very close, resulting in the highest possible colocalization. This was tried once but the secondary antibody did not survive the ExM protocol. Unexpected were the results of case II, since no colocalization was expected, but the Pearson coefficient was 0.45. This could suggest that GPIIb/IIIa forms clusters in resting platelets but will be discussed further in the discussion section.

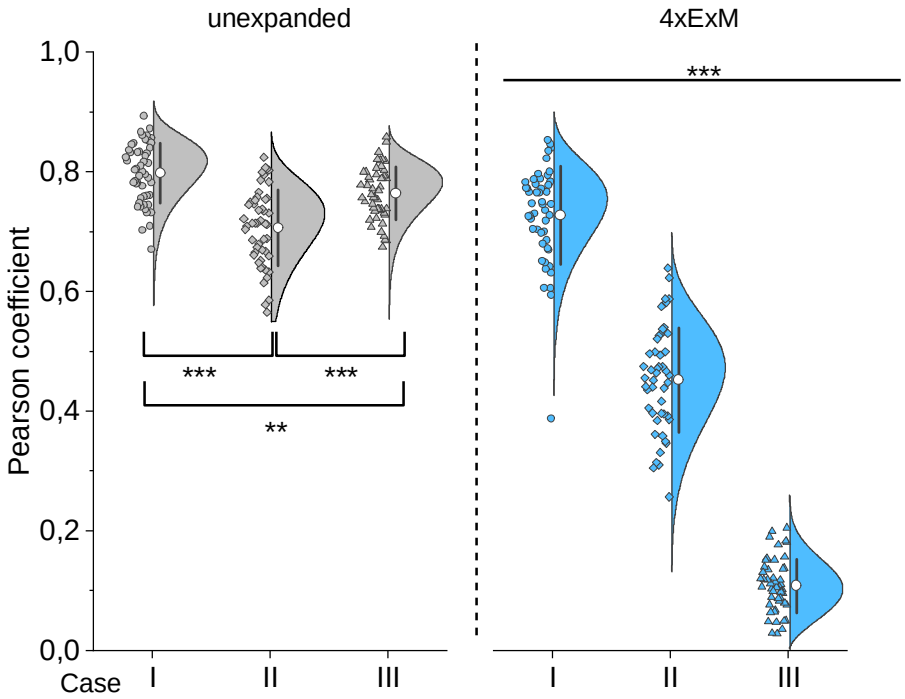

Figure 32: Results of the colocalization analysis. The expected Pearson coefficients were 1 for case I, 0 for cases II and III. The unexpanded samples (grey) show not a big difference between the mean values, whereas for the expanded samples (blue) a much bigger dynamic range is visible. Mean values: Case I: unexpanded: 0.79, expanded: 0.73. Case II: unexpanded: 0.71, expanded: 0.45. Case III: unexpanded: 0.76, expanded: 0.11. n = 50 for each case in expanded and unexpanded platelets. **: $p \leq 0.01$, ***: $p \leq 0.001$.

4 Summary & Discussion

Resolving membrane receptor distributions and interactions with fluorescence microscopy is challenging due to the small size and the high receptor density. Expansion microscopy (ExM), a novel technique which allows super-resolution using a diffraction limited microscope, could simplify and accelerate [55] the research on platelet membrane receptors because of its relatively easy protocol that solely relies on a novel procedure of sample preparation. Since ExM is a rather young technique, it's a fast improving field and new protocols and techniques are constantly published [28], [56]. One great asset of the ExM protocol lies in the ability to improve both, lateral and axial resolution, at the same level, but this requires a perfect isotropic expansion of the gel used. The use of ExM for platelet research is mainly limited by the signal loss due to the exposition of the fluorophores to digestive chemicals. This makes dim structures hard to preserve and detect. To analyze receptor interactions on the platelets membrane by colocalization analysis, it is required to adjust the ExM protocol to the platelet prerequisites to consequentially obtain the best image quality possible so that later the results can be validated using positive and negative control samples.

In this work, improvements have been made mostly regarding the signal intensity and I was able to demonstrate the potential of ExM in colocalization analysis. In the following, I will summarize which problems still exist, propose possible solutions and discuss the implications, potentials, and limitations of ExM with blood platelets.

Protocol optimization and use of different protocols

Protocol changes are the part which most influenced the results of the ExM experiments. However, both sample preparation and imaging have a big influence on the fluorescent intensity that can be achieved. Insufficient intensity results in low signal-to-noise levels, and eventually lower resolution and the intent to maximize the signal by increasing the illumination power and/or acquisition time is limited by photobleaching. Thus, preservation of fluorescence by proper sample preparation, is crucial. Here, signal loss is mainly caused by the digestion/denaturation step. I changed two substances compared to the original 4xExM protocol (fixation: PFA to Glyoxal and linking: Glutaraldehyde to Acryloyl-X), and the signal intensity in expanded samples increased significantly. Furthermore, unspecific signal, mainly produced by Glutaraldehyde, was reduced significantly and the platelets appearance as a hollow spherical cell was visible more clearly.

With the 10xExM protocol introduced by Truckenbrodt and co-authors [41], which allows a 10-fold expansion of the gel, first promising results have been achieved in this study, but the advantage and disadvantages over 4xExM needed to be carefully taken into account in the next steps. The higher signal loss due to more intensive digestion and higher volume increase (1000x instead of 64x in 4xExM) results in images with lower signal-to-noise levels, which could ruin the advantages of the resolution gain of a 10-fold expansion. Due to the ingredients in the 10xExM gel, its general consistency is much softer and vulnerable and often even varies from experiment to experiment. This poses the question if this inconsistency introduces variations in the expansion factors or even non-isotropic expansion. This could be controlled experimentally by imaging expanded DNA-origami structures. For the 10xExM protocol the oxygen content in the gel has a substantial negative influence on the gelation process, since it inhibits the polymerization process. A more efficient way to exclude oxygen from the gelation process would improve this consistency problem, although I have taken all precautions mentioned in the protocol to avoid this. A alternative approach could be to use a special sample chamber, which can be purged with nitrogen to completely eliminate oxygen from the reaction. Besides protocol-based problems, it is important to keep in mind that with 10-fold expanded samples comes a highly multiplied imaging time for each platelet, limiting the throughput of this method. To balance advantages and disadvantages of 10xExM it was necessary to compare the performance of 10xExM and 4xExM regarding data analysis like colocalization analysis to tell if the gain in resolution outweigh the disadvantages.

In contrast to the 4xExM and 10xExM protocol, the U-ExM protocol varies in the sequence of protocol steps and has different advantages and problems. The U-ExM protocol tackles the signal intensity problem by staining the sample when it is already linked to the gel and denaturated. Here, the fluorophores are not exposed to denaturation or digestion and therefore a high fluorescent intensity can be received. Nevertheless, before the staining step, the sample undergoes a denaturation step, during which the epitopes are fragmented and unfolded. This can grant access to new epitopes which have not been accessible before due to steric hinderance but also limits the choice of useable antibodies, since they need to bind specific sequences which can be found also after denaturation. Through the resemblance of the denaturation step to the method ‘Western Blot’, where samples are denaturated to detect specific proteins [57], in general antibodies, which can be used in Western Blot, should also

work in U-ExM. For CHO cells this worked with anti-tubulin antibodies, although it was not possible to image continuous microtubules. For platelets, antibodies which work in Western Blot were tried but it was not even possible to find the platelets in the gel, therefore it is likely that the antibodies could not attach to anything after denaturation. To verify this result and the antibody malfunction, it can be tested to add an anti-tubulin antibody as a control to locate the platelets in the sample.

Labeling strategy and potential use of other alternatives

Despite the improvements of the protocol, samples are rather dim and a further increase in signal intensity would be desirable in future. Unfortunately, the fluorophores we used (mostly Alexa488, 546 and 594) are those best retained during the ExM protocol according to Tillberg and co-authors. [37], so that we were at a limit here.

What also needs to be kept in mind is that we mostly used IgG antibodies, which during the expansion step increase the linkage error and consequently reducing the resolution gain reached through ExM (especially in 10xExM). The use of F_{ab}-Fragments would reduce this problem, because they are much smaller (~50 kDa vs. 150 kDa IgG antibodies [58]) since they consist only out of a fragment of an IgG antibody. Nevertheless, as the linkage error in ExM using IgG antibodies can be compared with other super-resolution methods [59], the use of F_{ab}-Fragments with the main disadvantage of very dim images due to a lower density of labeling is not implicitly necessary. Moreover, it is not clear, if F_{ab}-fragments are linked into the gel as reliable as IgG antibodies. With the introduction of a new labeling strategy as discussed below, this issue could be solved.

The introduction of a new labelling strategy could improve the signal intensity problem. A possible solution would be to use a trifunctional linker, as introduced by Wen and co-authors [60] or Shi and co-authors [61]. It would consist out of three domains: Antibody, Linker and Reporter (**Figure 33**). The linker itself is non-digestible and the fluorophore could be attached after the expansion over a Streptavidin to Biotin or an anti-Digoxigenin to Digoxigenin connection. With this method, the fluorophore is not exposed to digestion, what should result in better fluorophore preservation and therefore higher image contrast. Sophia Maier, who continued the project after me in the AG Heinze, successfully produced trifunctional linkers for platelet receptors and imaged platelets with superior contrast compared to regular IgG antibodies. Other approaches would be to try an additional labeling step after the gelation using a

secondary antibody to increase the intensity or to stain a second epitope on the same receptor (‘multi-epitope staining’), as done by Gao and co-authors [42]. They performed multi-epitope staining in combination with ExM and STED, this could be promising to use in ExM to increase the signal-to-noise ratio without suffering under strongly increased linkage error.

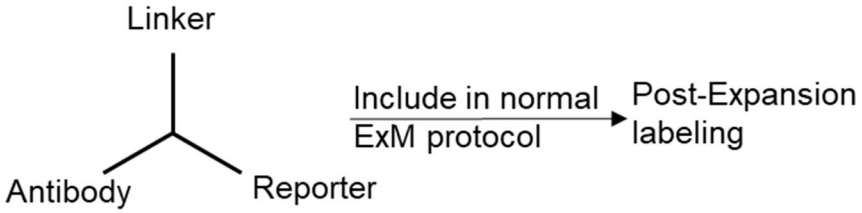

Figure 33: Trifunctional label as new labelling strategy. The trifunctional label consists out of three domains: Antibody (connects to the receptor), Linker (gets linked into the gel) and Reporter (binds a fluorophore). Advantages are that the label itself is not digested by Proteinase K and the fluorescent labelling takes place after expansion.

For simultaneous staining of intracellular proteins and membrane receptors, it was possible to show that Triton-X100 is too aggressive and does not allow staining of the membrane after permeabilization. The Glyoxal buffer, which we used as a fixative, showed permeabilizing effects which allowed staining of the cytoskeleton and the membrane at the same time without destroying the membrane, but this finding happened rather by chance and needs to be verified in further experiments.

Furthermore, in FACS analysis all available antibodies against the membrane receptors GPIX, GPIIb/IIIa, GPIbα/β were tested for different staining durations to see if it is possible to reduce the staining duration to reduce unspecific signal. Results showed that every antibody behaves differently regarding the increase of fluorescent intensity over longer staining durations. What can be generalized is, in live-staining, saturation is achieved very fast (no big intensity increase between 2 and 30 min staining duration), whereas for postfix-staining results are more variable and most antibodies show a big increase in fluorescent intensity between two and ten minutes, but also between ten and 30 minutes. In conclusion, staining duration is crucial and should be adjusted individually and carefully considering the used antibody.

Imaging

The imaging of platelets is challenging due to dim samples, which require high laser intensities for fluorescence excitation and long acquisition time, which makes the sample prone to photobleaching. I was able to determine microscope settings entailing

fast scanning (8000 Hz) and signal averaging that allow fast and effective imaging of stacks, which are important for quantitative analyses (Methods part 2.2.5 and 2.2.6/Appendix C). Still, imaging is an intensive procedure for the sample with almost total signal loss of the observed platelet after complete acquisition. Better preserved fluorescent intensity achieved through protocol changes would help to obtain better results.

For even higher resolutions, the combination of ExM and two super-resolution imaging methods were tested. First results showed that this combination is possible but delivered unexpected results. Theoretically Re-scanning microscopy (RCM) brings the advantages of higher sensitivity and faster imaging speed and a $\sqrt{2}$ times improved resolution compared to conventional confocal microscopy, but the images showed a much lower signal-to-noise ratio. The labeling density on the platelets seems to be so low that RCM cannot outperform confocal microscopy, probably due to the high noise level of the camera.

'Structured Illumination Microscopy' (SIM) did not work well on expanded platelets, because the low signal resulted in strong artefacts. With brighter samples, however, an additional resolution improvement of 2x could be achieved resulting in a final image resolution only accomplished by single molecule localization microscopy techniques at a >20x improvement in speed [55].

Towards resolving receptor distributions on blood platelets

Event count analysis

As already mentioned above, the ExM method does not provide a resolution high enough to image single molecules. Still, event counts for the different receptors could be analyzed and compared respectively their event count per surface. When comparing the event counts in samples which are stained for only GPIIb/IIIa (as shown in **Figure 31**) it is visible that Alexa488 appears to survive the ExM protocol worse than A546. This result matches with the findings of Tillberg and co-authors [37]. Furthermore, the results could be interpreted that the antibody 5D7 has a higher affinity to GPIIb/IIIa than 14A3 (**Figure 31**).

Colocalization analysis

Colocalization analysis is a tool that uses the spatial overlap of two fluorescent labels and helps to tell if two points can be allocated to the same structure or not. Hereby,

information about the relationship and interaction between objects can be obtained. In this study, colocalization analyses with different test scenarios were performed to study the performance of 4xExM regarding platelet receptors. When imaging two different receptors, a determined colocalization coefficient of 0 (= no colocalization) could be interpreted that the resolution is high enough to image the receptor distribution or that there are only few receptors on the membrane that hardly colocalize. Whereas a high colocalization coefficient can indicate colocalizing receptors or receptors which are too densely packed on the membrane to resolve them. In the test scenarios for the colocalization analysis in this work, membrane receptors were used which are highly abundant to avoid misinterpretations.

Table 3: Expected and Measured mean Pearson coefficients.

	Expectation	4xExM	unexpanded
Staining case I 14A3 (GPIIb/IIIa) 5D7 (GPIIb/IIIa)	1	0.73	0.79
Staining case II 14A3 (GPIIb/IIIa) 14A3 (GPIIb/IIIa)	0	0.45	0.71
Staining case III 56F8 (GPIX) 14A3 (GPIIb/IIIa)	0	0.11	0.76

Table 3 compares the expectations and measured results of the colocalization analysis within the three stainings cases. As already explained in 3.4.2, case I is the positive control and should show high colocalization with a high Pearson coefficient, while case II and IIII are negative controls and should show no colocalization with a low Pearson coefficient. The experiments showed that the use of 4xExM improved the dynamic range of the determined Pearson coefficient from 0.71 - 0.79 (conventional confocal microscopy) to 0.11 - 0.73 and hereby allows us to use it to make assumptions over colocalizing structures. For Staining case II, a Pearson coefficient of 0 was expected, but 0.45 was determined. The big gap between the two negative controls could be interpreted that GPIIb/IIIa forms clusters in resting platelets and therefore we see a higher Pearson coefficient as in the other negative control (case III). Otherwise, there is also four times less GPIX than GPIIb/IIIa in the platelets, what could also have influence on the low Pearson coefficient measured in Staining III. This effect could be eliminated by performing Colocalization analysis with two different receptors which are expressed at the same amount on the membrane.

As already mentioned in the theory part of this thesis, besides the Pearson's coefficient, there are other coefficients which describe colocalization like the Manders' coefficient. The Pearson coefficient is dependent from the number of colocalized pixels and takes the mean intensity of each channel in account. It is especially superior when imaging dim samples with different signal-to-noise levels and is not very vulnerable by fluorescent artefacts. Nevertheless, it fails when the number of events differs between the channels. The Manders' coefficient however is more sensitive to background noise but can calculate the colocalization of fractions of the two channels and obtains the colocalization coefficient in both directions. [45], [62]

As a follow-up study, experiments with expanded platelets and especially 10xExM were continued by Hannah Heil, Sophia Maier, Prateek Gupta and Luise Evers of the AG Heinze. Their results combined with my work have been published in Heil and co-authors in 2022 [59]. They startet to use the Manders' coefficient, since (as described before) it offers more stability regarding our specific platelet experiments. Using computer simulations, they calculated, that it is required to use 10xExM to reach a resolution which is sufficient for colocalization analysis of platelet receptors that are as abundant as for example GPIIb/IIIa. Therefore, the resolution gain achieved by using 4xExM is not sufficient to make proper statements about colocalization of platelet receptors. Consequently, they showed that colocalization experiments with 10xExM are feasible and results are superior compared to mine achieved with 4xExM when using the Manders' coefficient. Nevertheless 4xExM and 10xExM don't reach a resolution high enough to resolve single molecules and therefore there is a risk of detecting 'false positive' colocalizations [59]. Matching my results, in 10xExM they also obtained higher colocalizations for Staining case II as for case III, resuming that GPIIb/IIIa receptors 'are present in pre-formed clusters already on resting blood platelets', probably 'contributing to the rapid platelet responses upon vascular injury' [59].

5 Outlook

While there are many promising results, I have identified several bottlenecks that need to be addressed. Eventually a combination of tweaks and further analysis can help to fully exploit the potential of this technique. It is necessary to evaluate if the increased expansion factor in 10xExM really yields advantages, or if the image, and thus the resolution, suffers due to more intense digestion. By performing colocalization analysis using 10xExM, the results can be compared with 4xExM to show if 10xExM is superior and if the dynamic range of the colocalization coefficient can be amplified. Since the 10xExM protocol is more difficult to handle and therefore the results are more heterogeneous, the use of the 4xExM approach would keep the experiments easier (no need to exclude oxygen during the polymerization step) and the imaging much faster due to the much smaller imaging volume. Besides the use of 10xExM, the combination of ExM with other microscopy methods could bring further improvement regarding resolution, signal-to-noise ratio and imaging speed. A combination with Light sheet microscopy could be considered. Light sheet microscopy allows diffraction limited volumetric imaging with a high throughput and sensitivity by imaging a whole layer of the sample through illuminating it with a thin sheet of light [5]. A big issue of the ExM protocol is the labeling strategy. A library of successfully tested antibodies with ExM was created, but without exception the images are rather dim, and it is necessary to test new approaches for labeling. Promising is the use of trifunctional antibodies, which are equipped with three custom domains that can be equipped to the needs of the experiment and could ensure a better retention of the labels in the gel during washing and digestion steps. Furthermore, the use of this technique as shown by Shi and co-authors [61] could help to obtain much brighter images by attaching the fluorophore after the digestion step to the trifunctional label over a Streptavidin to Biotin bond. With this method, probably a well-performing antibody against GPIbα could be produced. The imaging of GPIbα together with the actin skeleton would be interesting, because, as mentioned before, the treatment of platelets with GPIbα leads to ‘non-classical’ clotting in *in vitro* experiments and their interaction with the actin skeleton is barely understood.

The results of my thesis show that the Expansion microscopy approach holds big potential for the blood platelet receptor research. Further experiments can profit from the high throughput of different samples with fast imaging and resolutions comparable to super-resolution microscopes.

Bibliography

[1] A. T. Franco, A. Corken, and J. Ware, “Platelets at the interface of thrombosis, inflammation, and cancer,” *Blood*, vol. 126, no. 5, pp. 582–588, 2015, doi: 10.1182/blood-2014-08-531582.

[2] D. Stegner and B. Nieswandt, “Platelet receptor signaling in thrombus formation,” *J. Mol. Med.*, vol. 89, no. 2, pp. 109–121, 2011, doi: 10.1007/s00109-010-0691-5.

[3] K. E. O’Connell *et al.*, “Practical murine hematopathology: A comparative review and implications for research,” *Comp. Med.*, vol. 65, no. 2, pp. 96–113, 2015.

[4] M. Zeiler, M. Moser, and M. Mann, “Copy Number Analysis of the Murine Platelet Proteome Spanning the Complete Abundance Range,” *Mol. Cell. Proteomics*, vol. 13, no. 12, pp. 3435–3445, 2014, doi: 10.1074/mcp.m114.038513.

[5] J. Vangindertael, R. Camacho, W. Sempels, H. Mizuno, P. Dedecker, and K. P. F. Janssen, “An introduction to optical super-resolution microscopy for the adventurous biologist,” *Methods and Applications in Fluorescence*, vol. 6, no. 2. IOP Publishing Ltd, Mar. 16, 2018. doi: 10.1088/2050-6120/aaae0c.

[6] M. G. L. Gustafsson, “Surpassing the lateral resolution limit by a factor of two using structured illumination microscopy,” *J. Microsc.*, vol. 198, no. 2, pp. 82–87, 2000, doi: 10.1046/j.1365-2818.2000.00710.x.

[7] M. J. Rust, M. Bates, and X. Zhuang, “Sub-diffraction-limit imaging by stochastic optical reconstruction microscopy (STORM),” *Nat. Methods*, vol. 3, no. 10, pp. 793–795, Oct. 2006, doi: 10.1038/nmeth929.

[8] F. Chen, P. W. Tillberg, and E. S. Boyden, “Expansion microscopy,” *Science (80-.).*, vol. 347, no. 6221, pp. 543–548, 2015.

[9] J. E. Italiano, S. Patel-Hett, and J. H. Hartwig, “Mechanics of proplatelet elaboration,” *J. Thromb. Haemost.*, vol. 5, no. SUPPL. 1, pp. 18–23, 2007, doi: 10.1111/j.1538-7836.2007.02487.x.

[10] J. J. Emeis, M. Jirouskova, E. M. Muchitsch, A. S. Shet, S. S. Smyth, and G. J. Johnson, “A guide to murine coagulation factor structure, function, assays, and genetic alterations,” *J. Thromb. Haemost.*, vol. 5, no. 4, pp. 670–679, 2007, doi: 10.1111/j.1538-7836.2007.02408.x.

[11] M. E. Daly, “Determinants of platelet count in humans,” *Haematologica*, vol. 96, no. 1, pp. 10–13, 2011, doi: 10.3324/haematol.2010.035287.

[12] M. Lebois and E. C. Josefsson, “Regulation of platelet lifespan by apoptosis,” *Platelets*, vol. 27, no. 6, pp. 497–504, 2016, doi: 10.3109/09537104.2016.1161739.

[13] A. D. Lopez and C. D. Mathers, “Measuring the global burden of disease and epidemiological transitions: 2002-2030,” *Ann. Trop. Med. Parasitol.*, vol. 100, no. 5–6, pp. 481–499, 2006, doi: 10.1179/136485906X97417.

[14] B. Savage, F. Almus-Jacobs, and Z. M. Ruggeri, “Specific synergy of multiple substrate-receptor interactions in platelet thrombus formation under flow,” *Cell*, vol. 94, no. 5, pp. 657–666, 1998, doi: 10.1016/S0092-8674(00)81607-4.

[15] D. Varga-Szabo, I. Pleines, and B. Nieswandt, “Cell adhesion mechanisms in platelets,” *Arterioscler. Thromb. Vasc. Biol.*, vol. 28, no. 3, pp. 403–413, 2008, doi: 10.1161/ATVBAHA.107.150474.

[16] B. Nieswandt and S. P. Watson, “Platelet-collagen interaction: Is GPVI the central receptor?,” *Blood*, vol. 102, no. 2. pp. 449–461, 2003. doi: 10.1182/blood-2002-12-3882.

[17] G. A. FitzGerald, “Mechanisms of platelet activation: Thromboxane A2 as an amplifying signal for other agonists,” *Am. J. Cardiol.*, vol. 68, no. 7, 1991, doi: 10.1016/0002-9149(91)90379-Y.

[18] B. Nieswandt *et al.*, “Long-term antithrombotic protection by in vivo depletion of platelet glycoprotein VI in mice,” *J. Exp. Med.*, vol. 193, no. 4, pp. 459–469, 2001, doi: 10.1084/jem.193.4.459.

[19] F. Nakamura *et al.*, “The structure of the GPIb-filamin A complex,” *Blood*, vol. 107, no. 5, pp. 1925–1932, 2006, doi: 10.1182/blood-2005-10-3964.

[20] W. Bergmeier, K. Rackebrandt, W. Schröder, H. Zirngibl, and B. Nieswandt, “Structural and functional characterization of the mouse von Willebrand factor receptor GPIb-IX with novel monoclonal antibodies,” *Blood*, vol. 95, no. 3, pp. 886–893, 2000, doi: 10.1182/blood.v95.3.886.003k45_886_893.

[21] E. Abbe, “Beiträge zur Theorie des Mikroskops und der mikroskopischen Wahrnehmung,” *Arch. Mikr. Anat.*, vol. 9, pp. 413–468, 1873, doi: 10.1007/BF02956173.

[22] R. Henderson and P. N. T. Unwin, “Three-dimensional model of purple membrane obtained by electron microscopy,” *Nature*, vol. 257, pp. 28–32, 1975, doi: 10.1038/257028a0.

[23] R. Henderson, J. M. Baldwin, T. A. Ceska, F. Zemlin, E. Beckmann, and K. H. Downing, “Model for the structure of bacteriorhodopsin based on high-resolution electron cryo-microscopy,” *J. Mol. Biol.*, vol. 213, no. 4, pp. 899–929, 1990, [Online]. Available: http://linkinghub.elsevier.com/retrieve/pii/S0022283605802712

[24] G. B. Airy, “On the Diffraction of an Object-glass with Circular Aperture,” *Trans. Cambridge Philos. Soc.*, vol. 5, pp. 283–291, 1835.

[25] J. W. Lichtman and J. A. Conchello, “Fluorescence Microscopy,” *Nature Methods*, vol. 2, no. 12. pp. 910–919, 2005. doi: 10.1002/9783527687732.ch3.

[26] G. M. R. De Luca *et al.*, “Re-scan confocal microscopy: scanning twice for better resolution,” *Biomed. Opt. Express*, vol. 4, no. 11, p. 2644, 2013, doi: 10.1364/boe.4.002644.

[27] E. Betzig *et al.*, “Imaging Intracellular Fluorescent Proteins at Nanometer Resolution,” vol. x, no. September, pp. 1642–1646, 2006.

[28] L. Schermelleh *et al.*, “Super-resolution microscopy demystified,” *Nat. Cell Biol.*, vol. 21, no. 1, pp. 72–84, 2019, doi: 10.1038/s41556-018-0251-8.

[29] T. A. Klar, S. Jakobs, M. Dyba, A. Egner, and S. W. Hell, “Fluorescence microscopy with diffraction resolution barrier broken by stimulated emission,” *Proc. Natl. Acad. Sci. U. S. A.*, vol. 97, no. 15, pp. 8206–8210, 2000, doi: 10.1073/pnas.97.15.8206.

[30] R. Y. Tsien, “The green fluorescent protein,” *Annu. Rev. Biochem.*, vol. 67, pp. 509–544, 1998, doi: 10.1146/annurev.biochem.67.1.509.

[31] I. C. Vreja *et al.*, “Super-resolution Microscopy of Clickable Amino Acids Reveals the Effects of Fluorescent Protein Tagging on Protein Assemblies,” *ACS Nano*, vol. 9, no. 11, pp. 11034–11041, 2015, doi: 10.1021/acsnano.5b04434.

[32] J. Ries, C. Kaplan, E. Platonova, H. Eghlidi, and H. Ewers, “A simple, versatile method for GFP-based super-resolution microscopy via nanobodies,” *Nat. Methods*, vol. 9, no. 6, pp. 582–584, 2012, doi: 10.1038/nmeth.1991.

[33] M. M. Harmsen and H. J. De Haard, “Properties, production, and applications of camelid single-domain antibody fragments,” *Appl. Microbiol. Biotechnol.*, vol. 77, no. 1, pp. 13–22, 2007, doi: 10.1007/s00253-007-1142-2.

[34] J. A. Cooper, “Effects of cytochalasin and phalloidin on actin.,” *J. Cell Biol.*, vol. 105, no. 4, pp. 1473–1478, 1987, doi: 10.1083/jcb.105.4.1473.

[35] K. N. Richter *et al.*, “Glyoxal as an alternative fixative to formaldehyde in immunostaining and super-resolution microscopy - Supplementary,” *EMBO J.*, vol. 37, no. 1, pp. 139–159, 2018, doi: 10.15252/embj.201695709.

[36] S. Truckenbrodt, C. Sommer, S. O. Rizzoli, and J. G. Danzl, “A practical guide to optimization in X10 expansion microscopy,” *Nat. Protoc.*, vol. 14, no. 3, pp. 832–863, 2019, doi: 10.1038/s41596-018-0117-3.

[37] P. W. Tillberg *et al.*, “Protein-retention expansion microscopy of cells and tissues labeled using standard fluorescent proteins and antibodies,” *Nat. Biotechnol.*, vol. 34, no. 9, pp. 987–992, 2016, doi: 10.1038/nbt.3625.

[38] T. J. Chozinski *et al.*, “Expansion microscopy with conventional antibodies and fluorescent proteins,” *Nat. Methods*, vol. 13, no. 6, pp. 485–488, Jun. 2016, doi: 10.1038/nmeth.3833.

[39] D. Gambarotto *et al.*, “Imaging cellular ultrastructures using expansion microscopy (U-ExM),” *Nat. Methods*, vol. 16, no. 1, pp. 71–74, 2019, doi: 10.1038/s41592-018-0238-1.

[40] J. B. Chang *et al.*, “Iterative expansion microscopy,” *Nat. Methods*, vol. 14, no. 6, pp. 593–599, 2017, doi: 10.1038/nmeth.4261.

[41] S. Truckenbrodt, M. Maidorn, D. Crzan, H. Wildhagen, S. Kabatas, and S. O. Rizzoli, “X10 expansion microscopy enables 25-nm resolution on conventional microscopes,” *EMBO Rep.*, vol. 19, no. 9, p. e45836, 2018, doi: 10.15252/embr.201845836.

[42] M. Gao *et al.*, “Expansion Stimulated Emission Depletion Microscopy (ExSTED).,” *ACS Nano*, vol. 12, no. 5, pp. 4178–4185, 2018, doi: 10.1021/acsnano.8b00776.

[43] Y. Wang *et al.*, “Combined expansion microscopy with structured illumination microscopy for analyzing protein complexes,” *Nat. Protoc.*, vol. 13, no. 8, pp. 1869–1895, 2018, doi: 10.1038/s41596-018-0023-8.

[44] Z. Tong, P. Beuzer, Q. Ye, J. Axelrod, Z. Hong, and H. Cang, “Ex-STORM: Expansion Single Molecule Super-resolution Microscopy,” *bioRxiv*, 2016, doi: 10.1101/049403.

[45] S. Bolte and F. P. Cordelières, “A guided tour into subcellular colocalization analysis in light microscopy,” *J. Microsc.*, vol. 224, no. 3, pp. 213–232, 2006, doi: 10.1111/j.1365-2818.2006.01706.x.

[46] K. W. Dunn, M. M. Kamocka, and J. H. McDonald, “A practical guide to evaluating colocalization in biological microscopy,” *Am. J. Physiol. Physiol.*, vol. 300, no. 4, pp. C723–C742, 2011, doi: 10.1152/ajpcell.00462.2010.

[47] S. Massberg *et al.*, “A crucial role of glycoprotein VI for platelet recruitment to the injured arterial wall in vivo,” *J. Exp. Med.*, vol. 197, no. 1, pp. 41–49, 2003, doi: 10.1084/jem.20020945.

[48] W. Bergmeier, V. Schulte, G. Brockhoff, U. Bier, H. Zirngibl, and B. Nieswandt, “Flow cytometric detection of activated mouse integrin αIIbβ3 with a novel monoclonal antibody,” *Cytometry*, vol. 48, no. 2, pp. 80–86, 2002, doi: 10.1002/cyto.10114.

[49] S. Ahmad, “Expansion Microscopy on Blood Platelets,” 2018.

[50] J. Schindelin *et al.*, “Fiji: An open-source platform for biological-image analysis,” *Nat. Methods*, vol. 9, no. 7, pp. 676–682, 2012, doi: 10.1038/nmeth.2019.

[51] M. Ovesný, P. Křížek, J. Borkovec, Z. Švindrych, and G. M. Hagen, “ThunderSTORM: A comprehensive ImageJ plug-in for PALM and STORM data analysis and super-resolution imaging,” *Bioinformatics*, vol. 30, no. 16, pp. 2389–2390, 2014, doi: 10.1093/bioinformatics/btu202.

[52] I. Arganda-Carreras, C. O. S. Sorzano, R. Marabini, J. M. Carazo, C. Ortiz-de-Solorzano, and J. Kybic, “Consistent and Elastic Registration of Histological Sections Using Vector-Spline Regularization,” *Comput. Vis. Approaches to Med. Image Anal.*, vol. 4241, 2006, doi: 10.1007/11889762_8.

[53] K. N. Richter *et al.*, “Glyoxal as an alternative fixative to formaldehyde in immunostaining and super-resolution microscopy,” *EMBO J.*, vol. 37, no. 1, pp. 139–159, 2018, doi: 10.15252/embj.201695709.

[54] S. Santoso, U. Zimmermann, J. Neppert, and C. Mueller-Eckhardt, “Receptor patching and capping of platelet membranes induced by monoclonal antibodies,” *Blood*, vol. 67, no. 2, pp. 343–349, 1986, doi: 10.1182/blood.v67.2.343.343.

[55] D. Mahecic, I. Testa, J. Griffié, and S. Manley, “Strategies for increasing the throughput of super-resolution microscopies,” *Curr. Opin. Chem. Biol.*, vol. 51, pp. 84–91, 2019, doi: 10.1016/j.cbpa.2019.05.012.

[56] P. W. Tillberg and F. Chen, “Expansion Microscopy: Scalable and Convenient Super-Resolution Microscopy,” *Annu. Rev. Cell Dev. Biol.*, vol. 35, no. 1, pp. 683–701, 2019, doi: 10.1146/annurev-cellbio-100818-125320.

[57] J. Renart, J. Reiser, and G. R. Stark, “Transfer of proteins from gels to diazobenzyloxymethyl-paper and detection with antisera: A method for studying antibody specificity and antigen structure,” *Proc. Natl. Acad. Sci. U. S. A.*, vol. 76, no. 7, pp. 3116–3120, 1979, doi: 10.1073/pnas.76.7.3116.

[58] P. J. Hudson and C. Souriau, “Engineered antibodies,” *Nat. Med.*, vol. 9, no. 1, pp. 129–134, 2003, doi: 10.1038/nm0103-129.

[59] H. S. Heil *et al.*, “Mapping densely packed αIIbβ3 receptors in murine blood

platelets with expansion microscopy," *Platelets*, vol. 33, no. 6, pp. 849–858, Aug. 2022, doi: 10.1080/09537104.2021.2023735.

[60] G. Wen *et al.*, "Evaluation of direct grafting strategies in Expansion Microscopy," *BioR*, pp. 1–12, 2019.

[61] X. Shi *et al.*, "Label-retention expansion microscopy," *bioRxiv*, p. 687954, 2019, doi: 10.1101/687954.

[62] E. Manders, F. Verbeek, and J. Aten, "Measurement of co-localization of objects in dual-colour confocal images," *J. Microsc.*, vol. 169, no. 3, pp. 375–382, 1993, doi: https://doi.org/10.1111/j.1365-2818.1993.tb03313.x.

Appendix

A. Fluorescence preserving properties of different fixation solutions

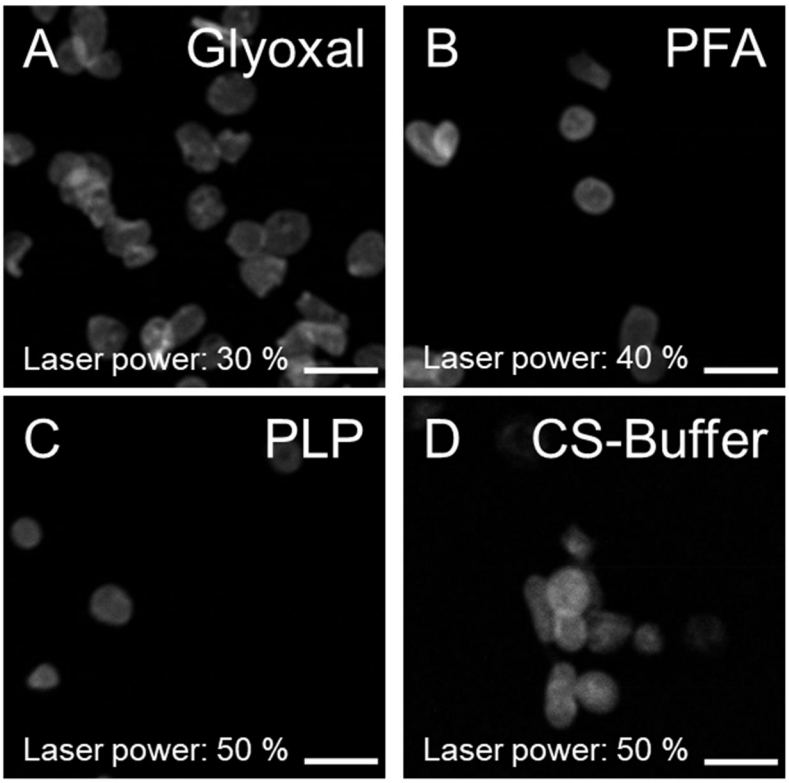

Figure 34: Comparison of fluorescence preserving properties of Glyoxal, PFA, PLP and CS-Buffer. Confocal images of not expanded platelets stained with anti-GPIX (56F8IgG-A594) and fixed with Glyoxal **(A)**, PFA **(B)**, PLP **(C)** and CS-Buffer **(D)**. The use of Glyoxal resulted in the brightest images with low laser power. Scale bar: 5 µm

B. Compatibility of different antibodies and Fab fragments against membrane receptors with ExM

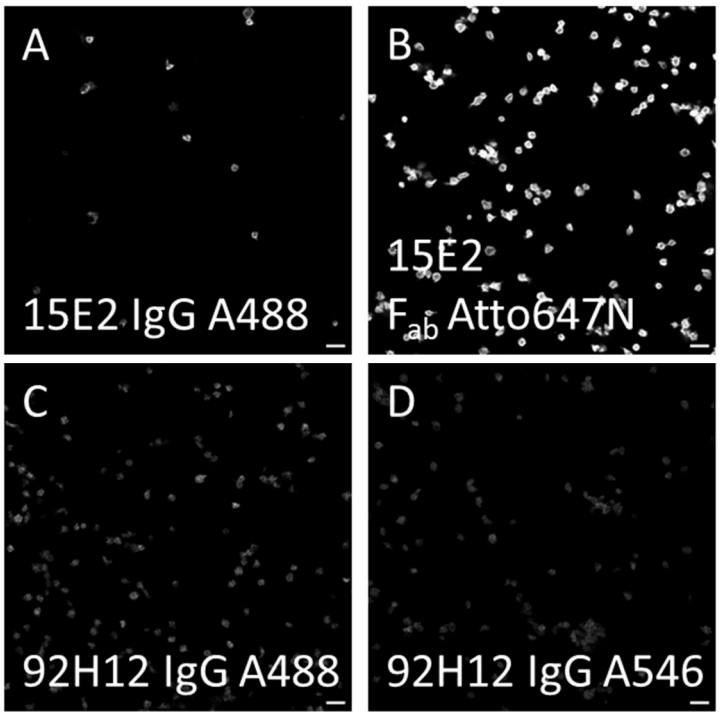

Figure 35: Intensity comparison in unexpanded platelets. IgG-Antibodies against GPIbα. Labeling: Post fixation. Scale bar: 5 µm. Laser power: 15 %

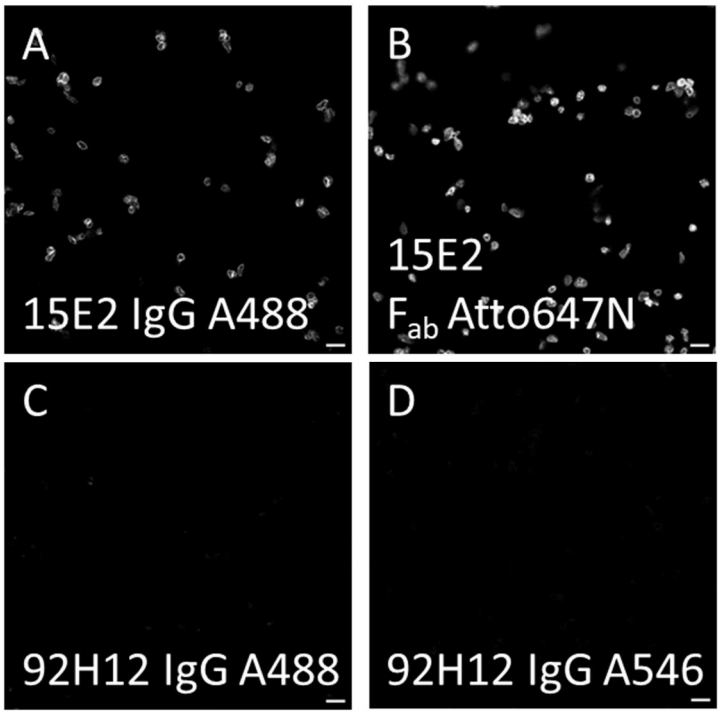

Figure 36: Intensity comparison in unexpanded platelets. IgG-Antibodies against GPIbα. Labeling:Live. Scale bar: 5 µm. Laser power: 15 %

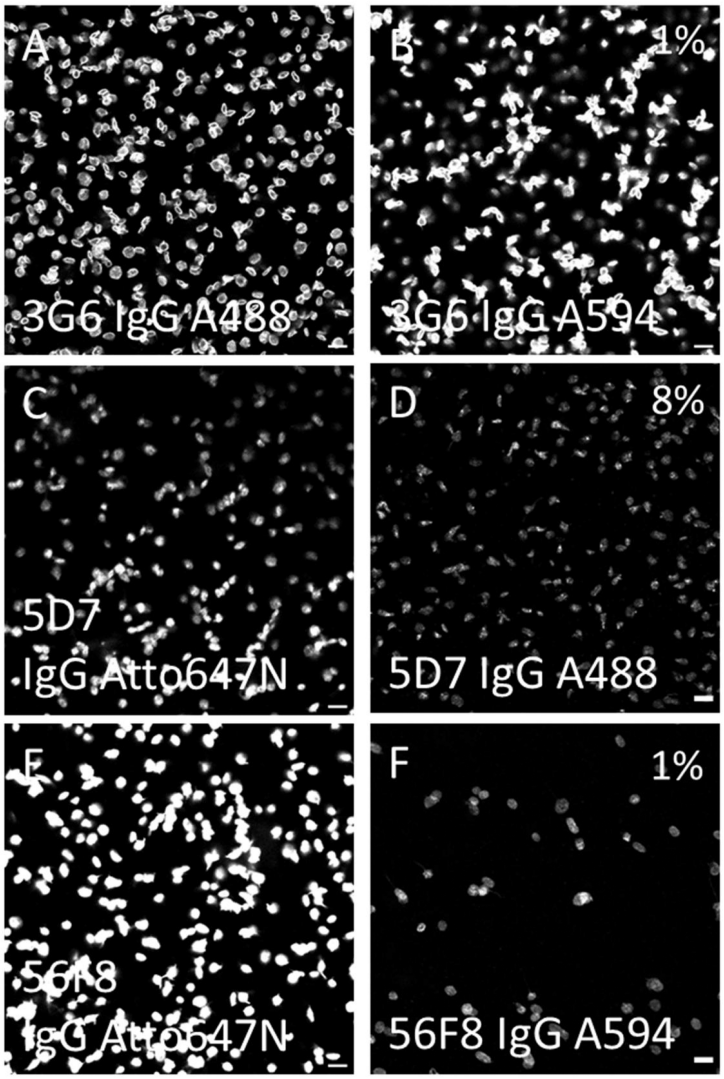

Figure 37: Intensity comparison in unexpanded platelets. IgG-Antibodies against GPIbβ (A+B), GPIIb/IIIa (C+D), GPIX (E+F). Labeling: Post-fixation. Scale bar: 5 µm. Laser power: A, C, E: 5 %; B, F: 1 %; E: 8 %

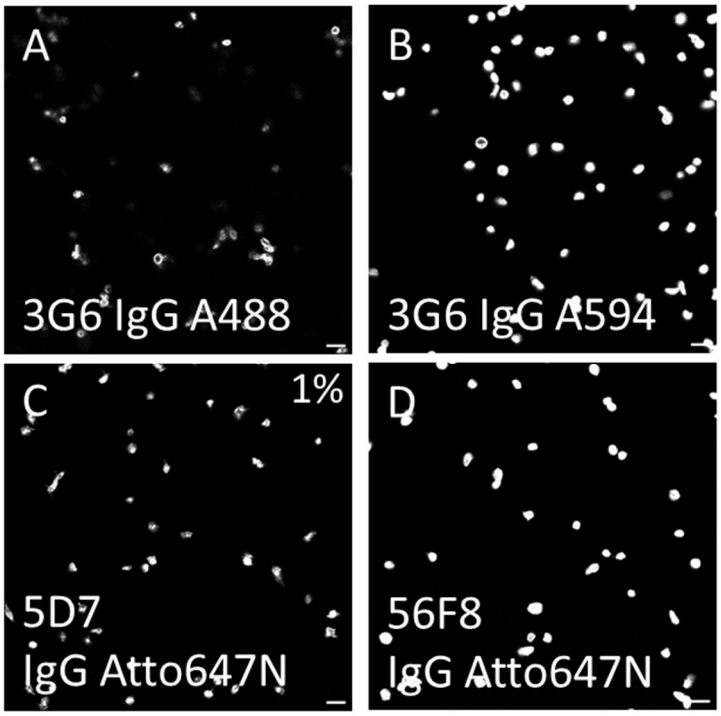

Figure 38: Intensity comparison in unexpanded platelets. IgG-Antibodies against GPIbβ (A+B), GPIIb/IIIa (C), GPIX (D). Labeling: Live. Scale bar: 5 µm. Laser power: A, B, D: 5 %; C: 1%

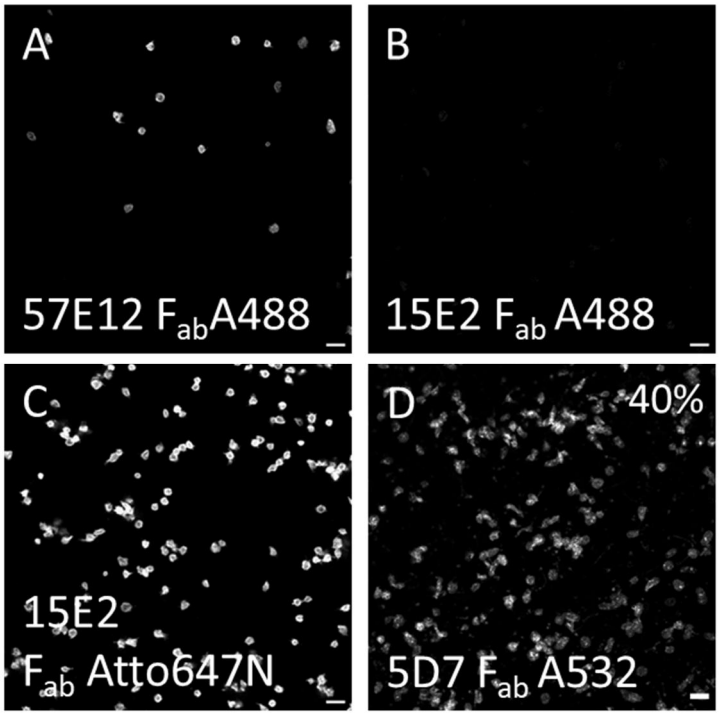

Figure 39: Intensity comparison in unexpanded platelets. F_{ab}-fragments against GPIbα (A+B+C), GPIIb/IIIa (D). Labeling: Post-fixation. Scale bar: 5 µm. Laser power: A, B, C: 15 %; D: 40 %.

C. Imaging Settings Colocalization Study

Unexpanded

Microscope	Leica SP5
Objective	HCX PL APO CS 63.0x1.20 WATER UV
Pinhole	1 AU
Scan Speed	8000 Hz
Pixels	1024 x 1024
Zoom	6
Line-Average	4
z-Step size	168 nm

Expanded

Microscope	Leica SP5
Objective	HCX PL APO CS 63.0x1.20 WATER UV
Pinhole	1 AU
Scan Speed	8000 Hz
Pixels	1024 x 1024
Zoom	6
Line-Average	4
z-Step size	168 nm

D. Statistics

Unexpanded platelets

Shapiro-Wilk-Test		p > 0.05
AnovaOneWay		p = 5.57E-14
2-tailed t-Test with Bonferroni correction	14A3+14A3 vs. 56F8+14A3	p = 2.13E-06
	14A3+5D7 vs. 14A3+14A3	p = 6.18E-12
	14A3+5D7 vs. 56F8+14A3	p = 1.80E-3

Expanded platelets

Shapiro-Wilk-Test	14A3+5D7	p =4.20E-4
	14A3+14A3	p = 0.94
	56F8+14A3	p = 0.47
Kruskal-Wallis		p = 3.4E-28
Mann-Whitney-Test with Bonferroni correction	14A3+5D7 vs. 14A3+14A3	p = 4.53E-22
	14A3+5D7 vs. 56F8+14A3	p = 2.36E-28
	56F8+14A3 vs. 14A3+14A3	p = 0

Acknowledgments

The herein presented work was performed in the group of Prof. Dr. Katrin Heinze at the Institute of Experimental Biomedicine, University Hospital and Rudolf Virchow Center, University Würzburg.

During the time of my thesis, many people supported me, and I gratefully thank the following people:

- Prof. Dr. Katrin Heinze for giving me the opportunity to do my medical doctors degree in her group, giving me the chance to gain experience in experimental research, always being available for questions
- Dr. Hannah Heil, especially for her full support which exceeded my actual time in the lab. Thank you for introducing me into this project, always being available for lots of questions, helping a lot with presentations or this thesis or simply turning off the oven when I forgot it.
- Dr. Vanessa Klaus, for sharing her knowledge about platelet preparation, giving me technical support, helping with experiments and proofreading this thesis.
- Prof. Dr. Markus Sauer and Prof. Dr. Harald Schulze, my thesis committee, for their support and advice.
- The Heinze Lab: Thank you very much to everybody for your help and support and the nice time.
- The Sauer Lab: Andreas Kurz and Fabian Zwettler, for letting me use the SIM and RCM setup and giving advice on the ExM protocol.
- Shazeb Ahmad, for showing me the protocol and the first steps of ExM in the lab.
- Lukas Weiß and Eva Aigner for proof-reading

Affidavit

I hereby confirm that my thesis entitled ‘Establishing successful protocols and imaging pipelines for Expansion Microscopy in murine blood platelets’ is the result of my own work. I did not receive any help or support from commercial consultants. All sources and / or materials applied are listed and specified in the thesis.

Furthermore, I confirm that this thesis has not yet been submitted as part of another examination process neither in identical nor in similar form.

Place, Date Signature

Eidesstattliche Erklärung

Hiermit erkläre ich an Eides statt, die Dissertation ‘Etablierung erfolgreicher Protokolle zur Probenpräparation und Bildgebung für die *Expansion Microscopy* in murinen Thrombozyten‘ eigenständig, d.h. insbesondere selbständig und ohne Hilfe eines kommerziellen Promotionsberaters, angefertigt und keine anderen als die von mir angegebenen Quellen und Hilfsmittel verwendet zu haben.

Ich erkläre außerdem, dass die Dissertation weder in gleicher noch in ähnlicher Form bereits in einem anderen Prüfungsverfahren vorgelegen hat.

Ort, Datum Unterschrift